PEOPLE'S DEMOCRATIC REPUBLIC OF ALGERIA
وزارة التعـليـم الـعالــي والـبحـث الـعلـمي
MINISTRY OF HIGHER EDUCATION AND SCIENTIFIC RESEARCH
جـامـعـة عمـــار ثـلـيـــجـــي بالأغـــواط
UNIVERSITY AMAR TELIDJI LAGHOUAT
كـلـيـــة الـعـلـــوم
FACULTY OF SCIENCES
قسم عـلـــوم المادة
DEPARTMENT OF MATERIAL SCIENCES

MASTER THESIS

DOMAIN: MATERIAL SCIENCES
FIELD: PHYSICS
OPTION: MATERIAL PHYSICS

by:

BOUZEKRI Oussama

Theoretical study of structural, electronic, optical and elastic properties of the ternary Zintl compounds A_2CuAs (A=Na, K)

Publicly defended before the jury consisting of:

Mr. HALIT Mohamed	Professor	President
Mr. BOUROUROU Yahia	MC	Examiner
Mr. MAABED Saïd	MA	Supervisor

2020-2021

Dedication

Dedicate this work to my precious parents,

To my beloved brothers and my dear sisters

Dedicate to all my wonderful teachers and professors

Dedicate to all my friends

Dedicate to …

ACKNOWLEDGEMENTS

*I thank above all **ALLAH** the Almighty who offered me will, patience and Health, allowing me to carry out this work. And I thank my parent.*

*First, I would like to express my deepest thanks to my supervisor **Mr. MAABED Said** who did me the honor to carry out this work under his direction, for his great patience, his availability and his judicious advice.*

*I thank jury president **Mr. HALIT Mohamed** and jury **Mr. BOUROUROU Yahia** for the interest which they brought to my initiation to research by agreeing to examine this work and enrich it with their proposals.*

I would also like to thank all the teachers, and a special mention of

***Mr. BOUCHENAFA Mohammed**, **Mr. BENGHIA Ali**, **Mr. CHERIET Abderahmane** and **Mr. ARAR Rabie**, …*

*I would like to take this opportunity to say warm thanks to **Mr. KHAMELOUL Fakhereddine**, **Mr. BOULEBDA Hichem** …*

TABLE OF CONTENTS

List of abbreviations

DFT: Density Functional Theory

DOS: Density of states

GGA: Generalized Gradient Approximation

GGA-PBE: Generalized Gradient Approximation Perdew-Burk-Ernzerhof

IZB: Irreducible zone of Brillouin

LDA: Local Density Approximation

LBFGS: Low memory-Broyden-Fletcher-Goldfarb-Shann

PDOS: Partial Density of States

PP: Pseudopotential (Pseudo-potential)

PW: Plane Wave

P.W: Wyckoff position

SCF: Self Consistent Field

TDOS: Total Density of States

ZB: Brillouin Zone

OFTG PP: On The Fly Generated Pseudopotential

EDD: Electron Density Difference

List of Figures

CHAPTER I

CHAPTER II

CHAPTER III

List of Tables

CHAPTER I

CHAPTER II

CHAPTER III

GENERAL INTRODUCTION

General Introduction

The rich solid-state chemistry of Zintl phases makes it a productive area for the discovery of new materials with complex crystal structures and fascinating physical characteristics. Usually, Zintl compounds are produced by a reaction between an electropositive element of group 1 (an alkaline) or of group 2 (an alkaline earth metal) with an electronegative element (transition metal or element of groups 13, 14, 15 or 16) (1).

This research is part of a wider inquiry of the not yet known physical properties of the ternary Zintl compounds A_2MPn (A=Li, Na, K; M=Cu, Ag, Au; Pn=P, As, Sb, Bi). Of particular interest, the ternary alkali metal coper pnictides A_2CuAs *(A=Na, K)* will be carefully investigated using state of the art first principle approaches.

Eisenmann et al (2; 3). produced the ternary alkali metal coper pnictides A_2CuAs *(A=Na, K)* as part of a lengthy list of polar intermetallic compounds. Despite the abundance of articles on the Zintl phases, there is a lack of research material published on these compounds. To the best of our knowledge, only their structural aspects have been studied (2; 3), leaving their physical properties unconsidered.

To fil the gap on the actual knowledge about the herein considered materials, this study attempts to gather data on their electronic structure, elastic properties and optical properties using reliable first principle methodologies. This is an opportunity to gather a lot of information and build a knowledge database on their physical characteristics that have not yet to be investigated. As a result, there are three objectives: First, to get more insight on known experimental results. Then, to elucidate the bonding processes, mechanical stability and the other ground state physical properties of these crystals, which could serve as guide for testing to generate predictions and stimulate consideration for new technological applications.

Now a days, it is possible to explore the structural, electrical, and dynamic properties of matter without having any prior experimental data on the material in issue thanks to simulations. Density Functional Theory (DFT), introduced by Hohenberg-Kohn (4) and Kohn-Sham (5), is now the most commonly utilized first principle theory in solid-state physics and materials science. DFT-based first-principle calculations, with some reasonable approximations, may anticipate ever more complicated materials and new interesting characteristics. On the other hand, comparing the results to current experiments allows the theoretical approaches to be confirmed.

In addition to a general introduction and a general conclusion, this work is divided into three chapters. The first is a review of the literature on Zintl phases. The crystal structure of the herein considered materials is given special consideration. The second chapter is divided into two sections:

1. The first section covers the fundamentals of density functional theory (DFT) and the approximations that are used to solve the Kohn-Sham equations. We also give an overview on the plane-wave technic (PW) and the pseudopotential approach (PP), as well as the CASTEP code.
2. The second section introduces some general knowledge on the elastic and optical properties, which will be useful later in our research.

The last chapter is devoted to the presentation and interpretation of the results of our calculations relating to structural, elastic, electronic and optical properties. These results were obtained using the methods described in the second chapter.

Finally, a summary of the major findings from this study is provided in a general conclusion.

References

1. **Kim, S.J., G.J. Miller, and J.D. Corbett.** *Zigzag chains of alternating atoms in A2AuBi (A= Na, K) and K2AuSb. Synthesis, structure, and bonding. Zeitschrift für anorganische und allgemeine Chemie.* s.l. : 636(1): p. 67-73, 2010.

2. **Eisenmann, B., G. Cordier, and H. Schäfer,.** *CaCuSb (Bi) und SrCuSb (Bi)-Ternäre Phasen im „aufgefüllten "NiAs-(Ni2In)-Typ/CaCuSb (Bi) and SrCuSb (Bi)-Ternary Phases in the „Filled "NiAs-(Ni2In)-Structure. Zeitschrift für Naturforschung* . s.l. : B, 29(7-8): p. 457-459., 1974.

3. **Wang, F.** *Rationalizing th structures of Zintl and polar intermetallic phases.* 2011.

4. **Hohenberg, P. and W. Kohn.** *Inhomogeneous electron gas.* 1964.

5. **Kohn, W. and L.J. Sham.** *Self-consistent equations including exchange and correlation effects. Physical review.* s.l. : 140(4A): p. A1133, 1965.

BIBLIOGRAPHIC REVIEW

I.1 Introduction

This part is a bibliographic study in which we will give an overview of some facts about the family of Zintl phases A_2BX, and then we will present a review on the ternary component A_2CuAs where A is *Na* or *K*.

I.2 Zintl Phases and polar intermetallic materials

I.2.1 Definition of Zintl Phases

In chemistry, a Zintl phase is the product of a reaction between an electropositive element of group 1 (an alkali) or group 2 (an alkaline-earthy) with an electronegative element (transition metal or an element of 13th to 16th group). Their name comes from the German chemist Eduard Zintl who was the first to systematically prepare and structurally characterize these phases in the 1930s. The term "Zintl Phase" was used for the first time by F. Laves in 1941. These phases are special classes (sub-group) of polar intermetallic that contain a block of electropositive elements and a block of electronegative elements. Schaefer, Eisenmann and Muller (1) proposed a more general definition where electron transfer for a Zintl phase is essentially complete between the alkaline or alkaline-earth cation and the electron-negative elements that attract electrons by covalent bonding or by formation of isolated pairs of electrons in such a way that they reach a filled valence layer. As a result, these phases have similar characteristics to salt from the ionic bond between the cationic and the anionic units. The anionic unit can be isolated anions and if there are not enough electrons for a full byte, they form covalent bonds and polyanionic units.

Typically, Zintl phases are compounds that: are fragile at high melting points, are diamagnetic or have temperature independent paramagnetic state, and are narrow gap semiconductors ($Eg<1eV$) (2; 1).

The Zintl concept provides a simple idea concerning the ionic and covalent bond in the intermetallic phases, allowing a simple description of the bond which gives an overview of the structure and properties of the Zintl phases.

I.2.2 Definition of polar intermetallic phases

The polar intermetallic phases and the Zintl phases have the same definition, but in general the difference in electronegativity between the electropositive and the electronegative components of these phases is smaller than in the Zintl phases. However, there is not a critical value of retaining that separates the Zintl phases from the polar intermetallic (3).

I.3 The Zintl compounds A_2CuAs (A=Na or K)

I.3.1 History

In 1974, Eisenmann et al. (4) Prepared and determined the crystal structure of new ternary compounds *ACuX* with (A=*Ca*, Sr, and X=*Sb*, *Bi*). These compounds are compatible with the *NiAs* (*Ni_2In*) structure. Two years later, they synthesized ternary compounds of general formula *A_2BX* where **A** is an alkaline metal, **B** is a transition metal and **X** is an element of the 15th group of the periodic table. They obtained three compounds, namely: *Na_2CuAs*, *K_2CuAs* and *K_2CuSb* (5). X-ray diffraction showed that they crystallized in the orthorhombic structure (pace group *Cmcm*) where the two elements **B** and **X** form a zigzag chain along the c axis. In 1977, Savelsberg and Schäfer (6; 7) have synthesized other new materials with the same structural properties, namely *K_2AgX* (X= *As*, *Sb* and *Bi*) and *Na_2CuP*. Then, in 1979, Schuster et al. (7) have prepared a new *Na_2AgSb* material. The structure of this compound contains *Ag-Sb* zigzag chains. After one year, Mues and Schuster (8) synthesized three other compounds: *Na_2AuAs*, *Na_2AuSb*, and *K_2AuSb*. The powder diffraction diagram showed that the *Na_2AuAs* and *Na_2AuSb* phases are compatible with the *Na_2CuAs* structure (9).

Table I.1 *Some materials from the A_2BX family.*

A_2BX	Space group (N °)	Structure	Z
Na_2AuAs (8)	Cmcm (63)	Orthorhombique	4
Na_2AuSb (8)	Cmcm (63)	Orthorhombique	4
Na_2AuBi (8)	Cmcm (63)	Orthorhombique	4
K_2AuSb (8)	Cmcm (63)	Orthorhombique	4
K_2AuBi (8)	Cmcm (63)	Orthorhombique	4
Na_2CuAs (5)	Cmcm (63)	Orthorhombique	4
K_2CuAs (5)	Cmcm (63)	Orthorhombique	4
K_2CuSb (5)	Cmcm (63)	Orthorhombique	4
Na_2AgAs (7)	$C222_1$ (20)	Orthorhombique	4
Na_2AgSb (7)	Cmcm (63)	Orthorhombique	4
K_2AgAs (6; 7)	$C222_1$ (20)	Orthorhombique	4
K_2AgBi (6; 7)	$C222_1$ (20)	Orthorhombique	4

To the best of our knowledge, very few theoretical studies are devoted to these compounds like that conducted by Wang in 2011 to rationalize their structure (3). Actually, there are no studies on

their electronic, optical and elastic properties. **Table I.1** provides an overview of materials belonging to this family.

I.4 Description of the crystallographic structure

The Zintl compounds A_2CuAs (A = *Na*, *K*) crystallize in:

- The orthorhombic structure (space group is *Cmcm* (N °: 63)).
- The multiplicity of the cell is (Z = 4). The conventional cell of this structure contains 16 atoms (8 atoms (of potassium *K* or sodium *Na*), 4 atoms of copper *Cu* and 4 atoms of arsenic *As*).

The arrangement of atoms is as follows:

- The potassium atoms *K* or *Na* occupy the 8g (x, y, 1/4) site, characterized by the two free x and y coordinates (are not fixed by the space group *Cmcm*).
- The copper atoms *Cu* occupy the site 4b (0, 1 / 2.0), in the middle of the stops in the plane (ab) of the conventional cell.
- The arsenic *As* atoms occupy the 4c (0, y, 1/4) site, characterized by the free y coordinate.

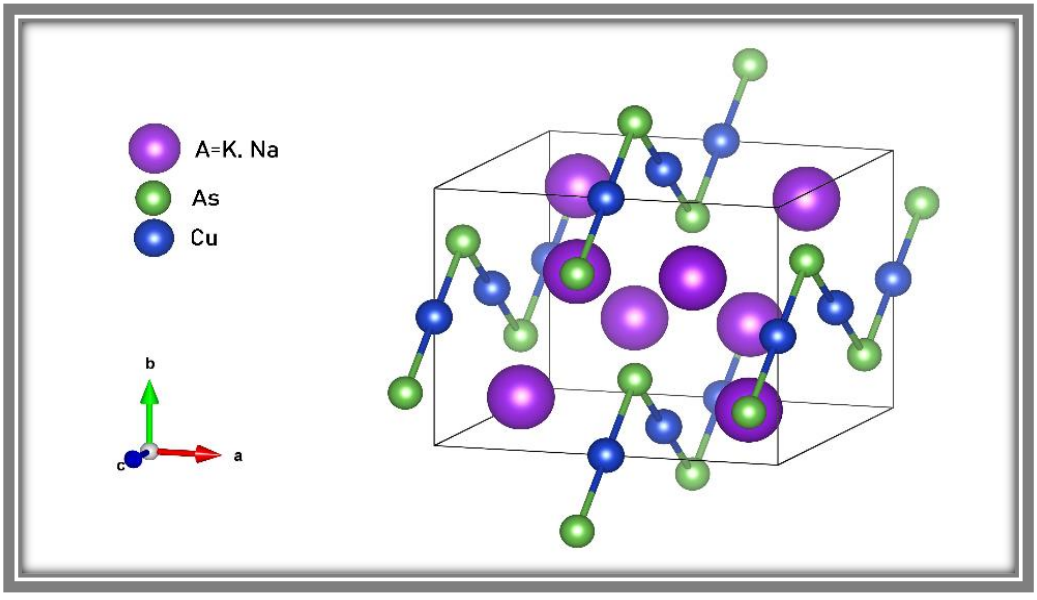

Figure I.1 *the orthorhombic structure (Cmcm) of K_2CuAs and Na_2CuAS.*

Table I.2 *The cell parameters of Na_2CuAs and K_2CuAs.*

Cell parameters (A°)	**K_2CuAs** (5)	**Na_2CuAs** (5)
a	10.020	8,860
b	7.560	7,220
c	5.890	7,220
α = β = γ	90°	90°

Table I.3 *The atomic positions of Na_2CuAs and K_2CuAs.*

Positions atomiques (Å)	**K** (5)	**Cu** (5)	**As** (5)	**Na** (5)	**Cu** (5)	**As** (5)
x	0.3315	0	0	0.3262	0	0
y	0.3543	0.50	0.261	0.3559	0.50	0.2343
z	0.25	0	0.25	0.25	0	0.25

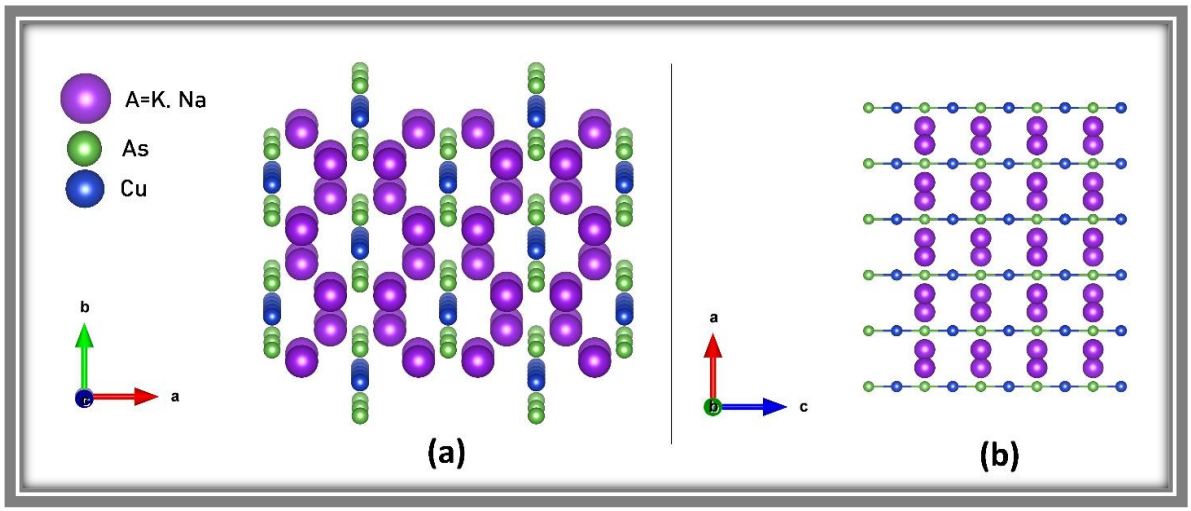

Figure I.2 *The Orthorhombic structure of Na_2CuAs and K_2CuAs: (a) seen along the c axis (b) seen along the b axis.*

The zigzag atomic chain consists of two double bonds (*Cu-As-Cu*) in which an angle of 108.2837° accrues at the Arsenic atom (**Figure I.3)**. The bond length (*Cu-As*) is 3.08450 Å (5).

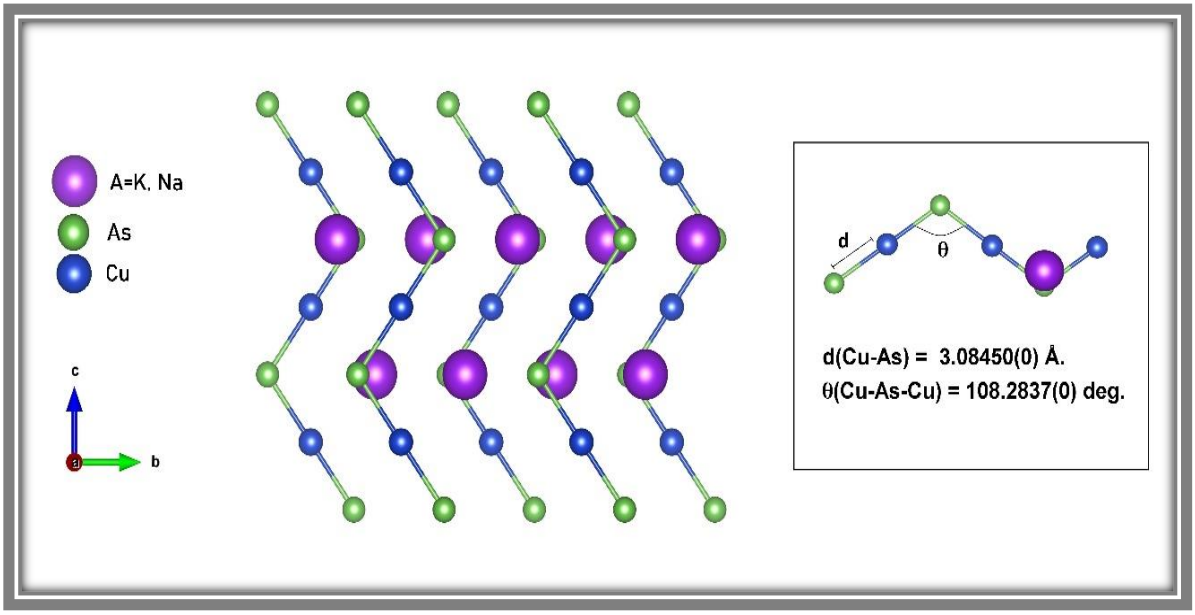

Figure I.3 *The zigzag chain Cu-Pn, the interatomic distances (Å), and the angle θ(°) for the compounds A_2CuAs (A = Na, K).*

I.5 Zintl phase applications

Actually, the Zintl border remain an active area, which has not been fully explored. The reasons lie both in the prerogatives for technological applications and the theoretical challenges raised - sometimes without conclusive answers - to explain the complexity of the Zintl crystal structures. Many Zintl phases exhibit new properties. These compounds are therefore promising for many applications, for example:

- Semiconductors.
- Thermoelectric materials.
- Improved magnetocaloric materials (2).

It is therefore important to study their unexplored physical properties to deduce potential new applications.

References

1. **I. Nandhakumar, N.White, S. Beeby.** *Thermoelectric materials and devices, Royal Society of Chemistry, RSC Energy and Environment Series 17, Gld,.* 2017.

2. **F. Appel, et al.** *., Intermetallic compounds–principles and practice. Progress, .* 2002. p. 617.

3. **Wang., F.** *Rationalizing th structures of Zintl and polar intermetallic phases.* 2011.

4. **Eisenmann, B., G. Cordier, H. Schäfer.** *CaCuSb (Bi) und SrCuSb (Bi)-Ternäre Phasen im „aufgefüllten "NiAs-(Ni2In)-Typ/CaCuSb (Bi) and SrCuSb (Bi)-Ternary Phases in the „Filled "NiAs-(Ni2In)-Structure. Zeitschrift für Naturforschung B.* 1974. pp. 457-459. Vols. 29(7-8).

5. **Eisenmann, B., G. Savelsberg, and H. Schäfer.** *Zur Darstellung und Kristallstruktur von Na2CuAs, K2CuAs und K2CuSb. Zeitschrift für Naturforschung B.* 1976. pp. 1344 -1346. Vol. 31(10).

6. **G. Savelsberg, H. Schäfer.** *Zeitschrift für Naturforschung B.* 1977. p. 745.

7. **Savelsberg, G., Schafer, H.** *Z. N aturforsch. Teil B.* 1978. p. 711. Vol. 33.

8. **H.-U. Schuster, C. Mues, W. Jung.** *Zeitschrift für Naturforschung B.* 1979. pp. 354 - 355.

9. **C. Mues, H.-U. Schuster.** *Zeitschrift für Naturforschung B.* 1980. p. 1055.

10. **Eisenmann, B., & Somer, M.** *Zeitschrift für Naturforschung B.* 1985. pp. 1419 - 1423. Vol. 40(11).

THE THEORETICAL FRAMEWORK

II.1 Introduction

Density functional theory (DFT) will be presented in this chapter. This approach is an effective tool for predicting and determining the physical and chemical properties of any material. It is mostly determined by the resolution of quantum mechanics equations, particularly the Schrödinger equation. However, except in extremely exceptional instances, the solution of this last equation remains extremely difficult and nearly impossible, leading to several rough estimations to aid in the resolution of this major problem.

II.2 The Schrödinger equation

For a solid body made up of a lot of interacting electrons and nuclei. The Schrödinger equation, which is time-independent and written as follows, describes physical properties (energy, electronics, optics, etc.) of this quantum system in its fundamental state (1).

$$H\Psi(r_i, R_\alpha) = E\Psi(r_i, R_\alpha) \qquad \text{(II. 1)}$$

In which:

- Ψ represents the wave function describing the state of the system.
- r_i the position vector of the electron $i = 1, 2, ...N_e$.
- R_α the position vector of the nucleus (ion) $\alpha = 1, 2, ...N_\alpha$.
- E his total energy.
- H represents the total Hamiltonian operator of the system given by the following relation:

$$H = T_e(r) + T_N(\mathrm{R}) + V_{ee}(r) + V_{Ne}(r, R) + V_{NN}(\mathrm{R}) \qquad \text{(II. 2)}$$

The Hamiltonian terms of the system are:

- $\hat{T}_e = \sum_{i=1}^{N_e} \hat{T}_i = \sum_{i=1}^{Ne} \left(\frac{-\hbar^2}{2m_i}\nabla_i^2\right)$ Is the total kinetic energy of electrons and m_i is the mass of the electron,
- $\hat{T}_N = \sum_{\alpha=1}^{N_\alpha} T_\alpha = \sum_{\alpha=1}^{N_\alpha} \left(\frac{-\hbar^2}{2M_\alpha}\nabla_\alpha^2\right)$ Is the total kinetic energy of the nuclei and M_α the mass of the nucleus,

- $\hat{V}_{ee} = \frac{1}{2}\sum_{i,j\neq i} \frac{e^2}{4\pi\varepsilon_0 \left|\vec{r}_i - \vec{r}_j\right|}$ Is the potential energy of the interaction between electrons,
- $\hat{V}_{NN} = \frac{1}{2}\sum_{\alpha,\beta\neq\alpha} \frac{Z_\alpha Z_\beta e^2}{4\pi\varepsilon_0 \left|\vec{R}_\alpha - \vec{R}_\beta\right|}$ Is the potential energy of the interaction between the nuclei,

  Z_α and Z_β are respectively the charges of the nuclei α and β,
- $\hat{V}_{eN} = -\sum_{i=1}^{N_e}\sum_{\alpha=1}^{N_\alpha} \frac{Z_N e^2}{4\pi\varepsilon_0 \left|\vec{R}_\alpha - \vec{r}_i\right|}$ Is the potential energy of the interaction electrons - nuclei.

We can write the Hamiltonian H in the form:

$$H = \left(\begin{array}{c} \sum_{i=1}^{N_e} \left(\frac{-\hbar^2}{2m_i}\nabla_i^2\right) + \sum_{\alpha=1}^{N_\alpha} \left(\frac{-\hbar^2}{2M_\alpha}\nabla_\alpha^2\right) + \frac{1}{2}\sum_{i,j\neq i} \frac{e^2}{4\pi\varepsilon_0 \left|\vec{r}_i - \vec{r}_j\right|} + \\ + \frac{1}{2}\sum_{\alpha,\beta\neq\alpha} \frac{Z_\alpha Z_\beta e^2}{4\pi\varepsilon_0 \left|\vec{R}_\alpha - \vec{R}_\beta\right|} - \sum_{i=1}^{N_e}\sum_{\alpha=1}^{N_\alpha} \frac{Z_N e^2}{4\pi\varepsilon_0 \left|\vec{R}_\alpha - \vec{r}_i\right|} \end{array} \right) \qquad \text{(II. 3)}$$

The atomic units (*Ua*) are used to simplify the formulation of equations. The following table describes these units:

Table II.1 *Atomic unit used in DFT and their equivalents in the international system (SI).*

Grandeur	Symbole	Unité (SI)	Unité atomique
Electron mass	Me	$9.1096\times 10^{-31}\,kg$	1ua
Electron charge	E	$-1.6022\times 10^{-19}\,C$	1ua
Length (Bohr radius)	$a_0 = \frac{4\pi\varepsilon_0\hbar}{m_e e^2}$	$5.2918\times 10^{-11}\,m$	1ua=1(Bohr)
Energy	$E_0 = \frac{\hbar^2}{m_e a_0}$	$4.359743\times 10^{-18}\,J$	1ua=1(Hartree)
Kinetic moment	$\hbar$	$1.0546\times 10^{-34}\,J/S$	1ua

The Schrödinger equation contains all of the observable features of the electron-nucleus system. To have access to the system's states and physical attributes, it is therefore sufficient to solve it. However, because it is a coupled wave function between all the particles, such an equation cannot

be solved rigorously. The number of particles increases the difficulty of this equation exponentially. As a result, in order to answer this problem, approximations have to be used. To begin, we'll look at Born-Oppenheimer's approximation.

II.3 The Born-Oppenheimer Approximation

The Born-Oppenheimer approximation (2) is the basis of many calculations in the physics of matter (3; 4). This approximation amounts to separating the movements of electrons from those of the nuclei. It is justified by the relatively high mass of nuclei compared to that of the electron (the mass of the proton is about 2000 times greater than that of the electron). Within the framework of this approximation, we study the movement of electrons in the mean field of supposedly fixed nuclei (5).

We write the wave function as a product of a nuclear wave function and an electronic wave function:

$$\Psi(\vec{R},\vec{r}) = \Psi_N(\vec{R})\Psi_e(\vec{r},\vec{R}) \qquad \text{(II. 4)}$$

And:

$$H = H_e + H_N \qquad \text{(II. 5)}$$

$$H_e = T_e + V_{ee} + V_{eN} \qquad \text{(II. 6)}$$

$$H_e = \left(\underbrace{\sum_{i=1}^{N_e} \left(\frac{-\hbar^2}{2m_i}\nabla_i^2\right) - \sum_{i=1}^{N_e}\sum_{\alpha=1}^{N_\alpha} \frac{Z_N e^2}{4\pi\varepsilon_0 \left|\vec{R}_\alpha - \vec{r}_i\right|}}_{h_i} + \frac{1}{2}\sum_{i,j\neq i} \frac{e^2}{4\pi\varepsilon_0 \left|\vec{r}_i - \vec{r}_j\right|} \right) \qquad \text{(II. 7)}$$

The electronic Schrödinger equation can then be written as follows:

$$H_e\Psi_e = E_e\Psi_e \qquad \text{(II. 8)}$$

The Born-Oppenheimer approximation is called adiabatic because it consists in separating the electronic problem from that network vibrations. This approximation significantly reduces the

degree of complexity this during the new wave function of the N-body dependent system, other additional approximations are required to be able to effectively solve this equation (6).

II.4 Hartree and Hartree-Fock approximation

In 1928, Hartree presented a second approximation. The assumption is that electrons travel independently of one another. That is, the probability of finding the coordinate electron r1 in orbital 1 is independent to the chances of obtaining other electrons.

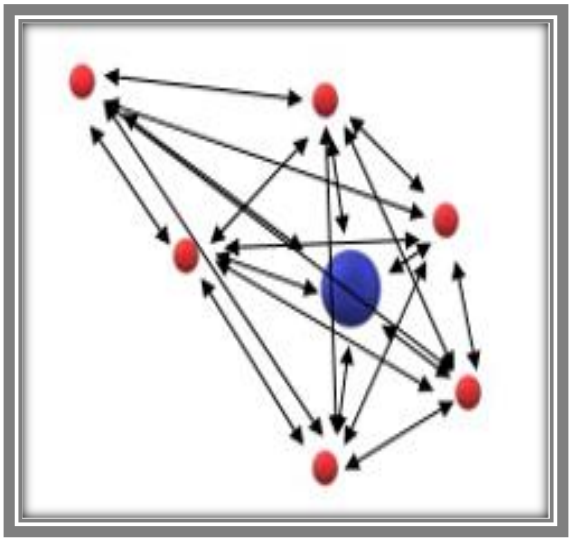

Figure II.1 *Many-electron systems. All electron-electron repulsion is included explicitly.*

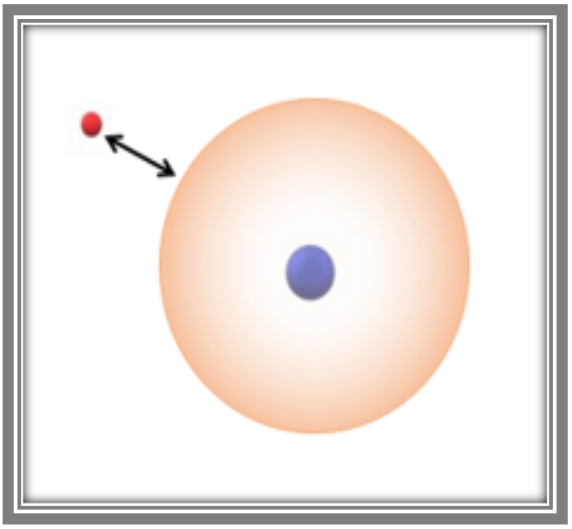

Figure II.2 *One-electron systems with remaining electron represented by an average charge density*

If we use this Hamiltonian to write out the Schrodinger equation for only one electron, the solutions will satisfy the eigen functions defined by this equation (7), which are known as spin orbitals.

$$H\Psi_i(r_i) = \varepsilon_i \Psi_i(r_i) \qquad \text{(II. 9)}$$

$$H_H = -\frac{\hbar^2}{2m}\Delta_i + V_{ext}\left(\vec{r},\vec{R}\right) + V_i^H\left(\vec{r}\right) \qquad \text{(II. 10)}$$

Where:

- $V_{ext}\left(\vec{r},\vec{R}\right)$ the potential due to the electron-nuclei interactions.
- $V_i^H\left(\vec{r}\right)$ the potential of Hartree associated with Coulomb interaction with other electrons.

The electronic wave function can therefore be expressed as a combination of electronic mono waves:

$$\Psi_e\left(r_1,r_2,...r_{Ne}\right)=\Psi_1(r_1)\times\Psi_2(r_2)...\times\Psi_{Ne}(r_{Ne}) \qquad \text{(II. 11)}$$

The energy of this wave function is the sum of the spin orbital energies:

$$\varepsilon_i=\varepsilon_1+\varepsilon_2+...\varepsilon_{Ne} \qquad \text{(II. 12)}$$

However, this approximation does not preclude two electrons from occupying the same quantum state because it is based on the concept of independent electrons and ignores the interaction of electrons with spin states. This goes against Pauli's exclusionary principle, which states that the wave function of a fermion system must be anti-symmetric when two particles are exchanged.

To remedy this, Hartree and Fock proposed that the multi electronic wave function be expressed by a Slater determinant:

$$\Psi^{HF}\left(x_1,x_2,\ldots.x_{Ne}\right)=\frac{1}{\sqrt{N}!}\begin{pmatrix}\Psi_1\left(x_1\right) & \Psi_2\left(x_1\right) & \cdots & \Psi_{Ne}\left(x_1\right)\\ \Psi_1\left(x_2\right) & \Psi_2\left(x_2\right) & \cdots & \Psi_{Ne}\left(x_2\right)\\ \vdots & \ddots & & \vdots\\ \Psi_1\left(x_{Ne}\right) & \Psi_2\left(x_{Ne}\right) & \cdots & \Psi_{Ne}\left(x_{Ne}\right)\\ & & & \end{pmatrix} \qquad \text{(II. 13)}$$

$\frac{1}{\sqrt{N}!}$ is here normalization constant, and where each wave function $\Psi^{HF}\left(x_1,x_2,\ldots.x_{Ne}\right)$ is called spin orbital, because it is composed of two parts: an orbital function and the other is a spin function (up or down),

Where $\frac{1}{\sqrt{N!}}$ is the normalization constant for this wave function, $\Psi^{HF}(x_1, x_2, \ldots .x_{Ne})$ denotes the mono-electron orbital spin, and x_i indicates the spatial and spin co-ordinates of the electron i grouped in the variable $x_i = \{r_i, \sigma_j\}$, $\Psi_i(x_i) \equiv \Psi_i(r_i, \sigma_j)$.

Orbital spins are given by the product of an orbital function $\Psi_i(r_i)$ is a spin function $\alpha(\sigma_j)$ where $\sigma = \pm\frac{1}{2}\begin{cases} spin\ \alpha(\uparrow)\ \sigma=\frac{1}{2} \\ spin\ \beta(\downarrow)\ \sigma=-\frac{1}{2} \end{cases}$ The spin functions and obey the orthonormality condition:

$$\langle\alpha|\alpha\rangle = \langle\beta|\beta\rangle = 1 \text{ et } \langle\alpha|\beta\rangle = \langle\beta|\alpha\rangle = 0 \qquad \text{(II. 14)}$$

Slater's determinant satisfies the principle of antisymmetric because it changes sign if we swap two rows or two columns. Swapping two lines is like changing the space and spin coordinates of pairs of electrons. We therefore have the property of antisymmetric with respect to this exchange (8).

$$\left[\left(-\frac{1}{2}\nabla_i^2 + V_{ext}(\vec{r},\vec{R}) + \sum_{i\neq j=1}^{Ne}\int\frac{\left|\varphi_j(\vec{r}')\right|^2}{\left|\vec{r}-\vec{r}'\right|}d\vec{r}'\right)\varphi_j(\vec{r}') + \sum_{i\neq j=1}^{Ne}\int\frac{\varphi_j(\vec{r})\varphi^*{}_j(\vec{r}')}{\left|\vec{r}-\vec{r}'\right|}d\vec{r}'\varphi_j(\vec{r}')\right] = \varepsilon_i\varphi_i(\vec{r}) \qquad \text{(II. 15)}$$

- $-\frac{1}{2}\nabla_i^2$ The kinetic energy of the electron i.
- $V_{ext}(\vec{r},\vec{R})$ The energy of attraction between nuclei and electrons.
- $\sum_{i\neq j=1}^{Ne}\int\frac{\left|\varphi_j(\vec{r}')\right|^2}{\left|\vec{r}-\vec{r}'\right|}d\vec{r}'$ The integral of Coulomb noted (the potential of Hartree).
- $\sum_{i\neq j=1}^{Ne}\int\frac{\varphi_j(\vec{r})\varphi^*{}_j(\vec{r}')}{\left|\vec{r}-\vec{r}'\right|}d\vec{r}'\varphi_j(\vec{r}')$ The exchange integral.

We fix the positions of the atomic nuclei in a Hartree–Fock (HF) calculation with the aim of determining the wave function of Ne interacting electrons.

II.5 Density functional theory (DFT)

Density functional theory (DFT) is one of the most effective and widely used quantum mechanical methods for describing matter today. It can be applied to atoms, molecules, and solids, as well as quantum and classical fluids. Indeed, DFT is now commonly used in chemistry to calculate a wide range of properties (e.g., molecular structures, reaction paths, etc.) and in physics (e.g., band structures of solids) (1).

The basic concept of density functional theory was established in the 1920s with Thomas and Fermi's work on the uniform electron gas (9; 10), which proposed that a system's energy is fully determined by its electron density. However, it wasn't until 1964 that the Hohenberg and Kohn (H-K) theorems (11) and the derivation of the set of mono-electronic equations that can be used to obtain the ground state density (Kohn-Sham equations) (12) were written.

II.5.1 Thomas –Fermi approximation

In 1927, it was proposed to replace the wave function with the charge density (9), resulting in the so-called Thomas–Fermi approach to electronic structure. By adding a concept to describe the exchange energy, Dirac strengthened the theory (12).

The total energy of the system is written as:

$$E_{TF} = \left[\begin{array}{l} C_1 \int \rho(\vec{r})^{5/3} d\vec{r} + \int V_{ext}(\vec{r}) \rho(\vec{r}) d\vec{r} + \\ + C_2 \int \rho(\vec{r})^{4/3} d\vec{r} + \frac{1}{2} \int \frac{\rho(\vec{r}) \rho(\vec{r}')}{|\vec{r} - \vec{r}'|} d\vec{r} d\vec{r}' \end{array} \right] \qquad \text{(II. 16)}$$

With $C_1 = (3/10)(3\pi^2)^{2/3}$ and $C_2 = -(3/4)(3/\pi)^{1/3}$. The kinetic energy is described first, followed by the electron–nuclei interaction, the exchange, and finally the Hartree term. The kinetic energy and correlation terms of the many-electron system are derived in the expression above assuming a homogenous electron gas (HEG). Because the HEG is so important in DFT, we'll repeat its definition here and also the definition of the often-used parameters. The density ρ of the homogeneous electron gas is:

$$\rho = \frac{n}{\Omega} \qquad \text{(II. 17)}$$

Where *n* is the total number of electrons in the volume Ω

Although the Thomas–Fermi theory did not provide any quantitatively impressive findings, the basic idea of employing the electron charge density as the basic variable rather than the wave function proved to be extremely beneficial.

II.5.2 The Hohenberg-Kohn (HK) theorems

In 1964, the concept of the Thomas–Fermi method was revived by the so-called Hohenberg–Kohn theorem (13). This approach is based on two theorems:

Theorem 1:

The electronic density $\rho(r)$ is the single function required to derive all of a system's attributes. In other words, the electrical density of the ground state $\rho_0(r)$ and the external potential $V_{ext}(r)$, and hence $\rho_{fond}(r)$ and the ground state wave function Ψ_{fond}, have a one-to-one connection.

$$E = E\left[\left(\rho_{fond}\right)\right] = F_{HK}\left[\left(\rho_{fond}\right)\right] + \int V_{ext}(r)\rho(r)dr \qquad \text{(II. 18)}$$

With:

$$F_{HK}\left[\left(\rho_{fond}\right)\right] = T\left[\rho(r)\right] + V_{ee}\left[\rho(r)\right] \qquad \text{(II. 19)}$$

Where:

- $V_{ee}\left[\rho(r)\right]$ is the term of electron-electron interactions.
- $T\left[\rho(r)\right]$ is the kinetic energy of the electronic system.
- $F_{HK}\left[\left(\rho_{fond}\right)\right]$ The functional of Hohenberg and Kohn.

The first theorem does not provide us with enough information to decide whether or not a given density is that of the ground state. This is the subject of Hohenberg and Kohn's second theorem.

Theorem 2:

The energy functional $E[\rho]$ is minimal when any electronic density $\rho(r)$ equals the electronic density of the ground state $\rho_{fond}(r)$, according to this theorem.

$$E\left[\rho_{fond}\right] = MinE[\rho] \qquad \text{(II. 20)}$$

That is, a test electron density ρ_{test} defines its own Hamiltonian and test wave function Ψ_{test}, according to the first theorem. From there, we can establish a correlation between the variationnel principle in its wave function version and electronic density versions, as follows:

$$\left\langle \Psi_{test} \middle| H \middle| \Psi_{test} \right\rangle = E\left[\rho_{test}\right] \geq E_{fond} = \left\langle \Psi_{fond} \middle| H \middle| \Psi_{fond} \right\rangle \qquad \text{(II. 21)}$$

In summary, the electronic density of the ground state can be used to identify all of the features of a system specified by an external potential V_{ext}. If and only if the electronic density is that of the ground state, the energy of the system $E(r)$ reaches its minimal value.

However, rewriting a precise analytical formulation of the functional $F_{HK}[\rho]$ for an interacting **N** electron system remains a big challenge.

- $V_H(r)$ the electronic potential of Hartree which is expressed by:

$$V_H(r) = \frac{e^2}{2}\int \frac{n(r)n(r')}{|r-r'|} d^3r d^3r' \qquad \text{(II. 22)}$$

- $V_{XC}(r)$ the potential of exchange and correlation obtained by the simple derivative of the exchange energy and correlation with respect to the electronic density:

$$V_{XC}(r) = \frac{\partial E_{XC}\left[n(r)\right]}{\partial n(r)} \qquad \text{(II. 23)}$$

As each electron goes through the effect of the effective potential V_{eff} created by all other electrons, the equations of Kohn and Sham become:

$$H\Psi_i = \left[\frac{\hbar^2}{2m} \nabla^2 + V_{eff}(r) \right] \Psi_i = E_i \Psi_i \qquad \text{(II. 24)}$$

II.5.3 Kohn-Sham equations

The interacting multi-particle physical system is substituted with a fictitious system of independent particles, which is easier to solve, according to Kohn and Sham. They assumed that the electron density of the real system's ground state is the same as the fictional systems.

This results in the solution of a set of equations for independent particles, such as the Hartree or Hartree-Fock equations:

$$H_{KS}\Psi_i(\vec{r}) = \varepsilon_i \Psi_i(\vec{r}) \qquad \text{(II. 25)}$$

With:

$$H_{KS} = -\frac{1}{2}\nabla_i^2 + V_{eff}(\vec{r}) \qquad \text{(II. 26)}$$

And:

$$V_{eff} = V_{ext}(\vec{r}) + \underbrace{\int \frac{n(\vec{r}')}{|\vec{r} - \vec{r}'|} dr'}_{V_H(\vec{r})} + V_{XC}(\vec{r}) \qquad \text{(II. 27)}$$

Where:

- $V_{ext}(\vec{r})$ is extern potential.
- $V_H(\vec{r})$ is Hartree potential.
- $V_{XC}(\vec{r})$ is exchange and correlation potential.

The issue is that we can't handle the exchange and correlation energy precisely, so we have to make estimates.

II.6 The exchange and correlation functional

II.6.1 Local density approximation (LDA)

Assume that the electron density at a point r is depends only on the density in r and equal to the correlation energy per particle of a homogeneous gas with density n(r):

$$E_{XC}^{LDA}\left[n(\vec{r})\right]=\int n(\vec{r})\,\varepsilon_{XC}^{LDA}\left[n(\vec{r})\right]d\vec{r} \qquad \text{(II. 28)}$$

The exchange-correlation energy can also be broken down into the sum of the exchange and correlation energies.

$$\varepsilon_{XC}^{LDA}\left(n(\vec{r})\right)=\varepsilon_{X}\left[n(\vec{r})\right]+\varepsilon_{C}\left[n(\vec{r})\right] \qquad \text{(II. 29)}$$

The term exchange energy is known; it is given by functional energy exchange of Thomas-Fermi-Dirac:

$$E_{XC}^{GGA}\left[n(\vec{r}),\nabla n(\vec{r})\right]=\int n(\vec{r})\,\varepsilon_{XC}^{GGA}\left[n(\vec{r}),\nabla n(\vec{r})\right]dr \qquad \text{(II. 30)}$$

On the other hand, the correlation energy, which is more complex to evaluate, is assessed via quantum Monte Carlo-methods (14).

II.6.2 Generalized Gradient Approximation (GGA)

The LDA method assumes a uniform electron density because it is based on the homogeneous electron's gas model. However, atomic or molecular systems are rarely identical to a homogeneous electron gas; in a broader sense, all genuine systems are inhomogeneous, which means that the electronic density varies spatially (locale) (15).

The majority of the corrections implemented at the LDA are based on the concept of accounting for local density differences. As a result, the electronic density gradient has been included, leading to the generalized gradient approximation (GGA), in which the exchange-correlation energy is dependent on the electron density and its gradient:

$$E_{XC}^{GGA}\left[n(\vec{r}),\nabla n(\vec{r})\right]=\int n(\vec{r})\,\varepsilon_{XC}^{GGA}\left[n(\vec{r}),\nabla n(\vec{r})\right]dr \qquad \text{(II. 31)}$$

There are many expressions to describe the GGA functional following the choice of $\varepsilon_{XC}\left[n(\vec{r}),\nabla n(\vec{r})\right]$ as forms of Becke (B88) (16). from Perdew-Wang (PW91) (17) and Perdew-Burke- Ernzerhof (PBE) (18) Hansen and Norskov (RPBE) (19).

II.6.3 Hybrid Functional

The inclusion of LDA or GGA in DFT calculations provides for a more precise description of energy-related physical parameters including equilibrium geometry and elastic characteristics. However, when computing the ground state energy of tiny molecules and the semiconducting band gaps for extended systems, these two approaches still produce considerable inaccuracies.

A new generation of exchange-correlation functional has recently been designed to compensate for these problems. The exchange-correlation energy functional in these models combines Hartree-Fock and other DFT formalisms (LDA or GGA). PBE0, HSE03, HSE06, and B3LYP are the most frequent hybrid functional at the moment (20). The employment of such functional allows for exact reproduce of experimental results.

Hybrid functional are very useful for describing molecules, insulators, semiconductors, and transition metal oxides in general. Their main disadvantage is that, due to the inclusion of Hartree-Fock components, such calculations are computationally more expensive than standard functional.

II.6.4 Solving the equations of kohn-sham

To solve the Kohn-Sham equations, one must first choose a basis set for the wave functions that can be expressed as a linear combination of orbitals, known as Kohn-Sham orbitals (KS) written in the form:

$$\Psi_i(\vec{r}) = \sum C_{ij}\Phi_j(\vec{r}) \qquad \text{(II. 32)}$$

Where $\Phi_j(\vec{r})$ are the basis functions and C_{ij} the development coefficients.

The calculation of the coefficients C_{ij} for occupied orbitals that minimize the total energy is the key to solving the Kohn and Sham equations. The calculations are made easier by resolving the KS equations for symmetry sites in the first Brillouin zone. As shown in the flowchart of Figure, this resolution is accomplished in an iterative manner using an auto coherent iteration cycle (II.1). To diagonalizable the secular equation, we start by infusing the initial charge density ρ_{in} :

$$(H_{\varepsilon i}S)C_i = 0 \qquad \text{(II. 33)}$$

Where H represents the Hamiltonian matrix and S the overlay matrix. The overall charge density that may be derived by summation over all occupied orbitals is then used to generate the new charge density ρ_{out} using the eigenvectors of this secular equation.

If the calculations do not match, the two densities ρ_{in} and ρ_{out} are mixed in the following way:

$$\rho_{in}^{i+1} = (1-a)\,\rho_{in}^{i} + a\rho_{out}^{i} \qquad \text{(II. 34)}$$

i represents the i^{th} iteration and α is a mixing parameter. Thus, the iterative procedure can be continued until convergence is achieved.

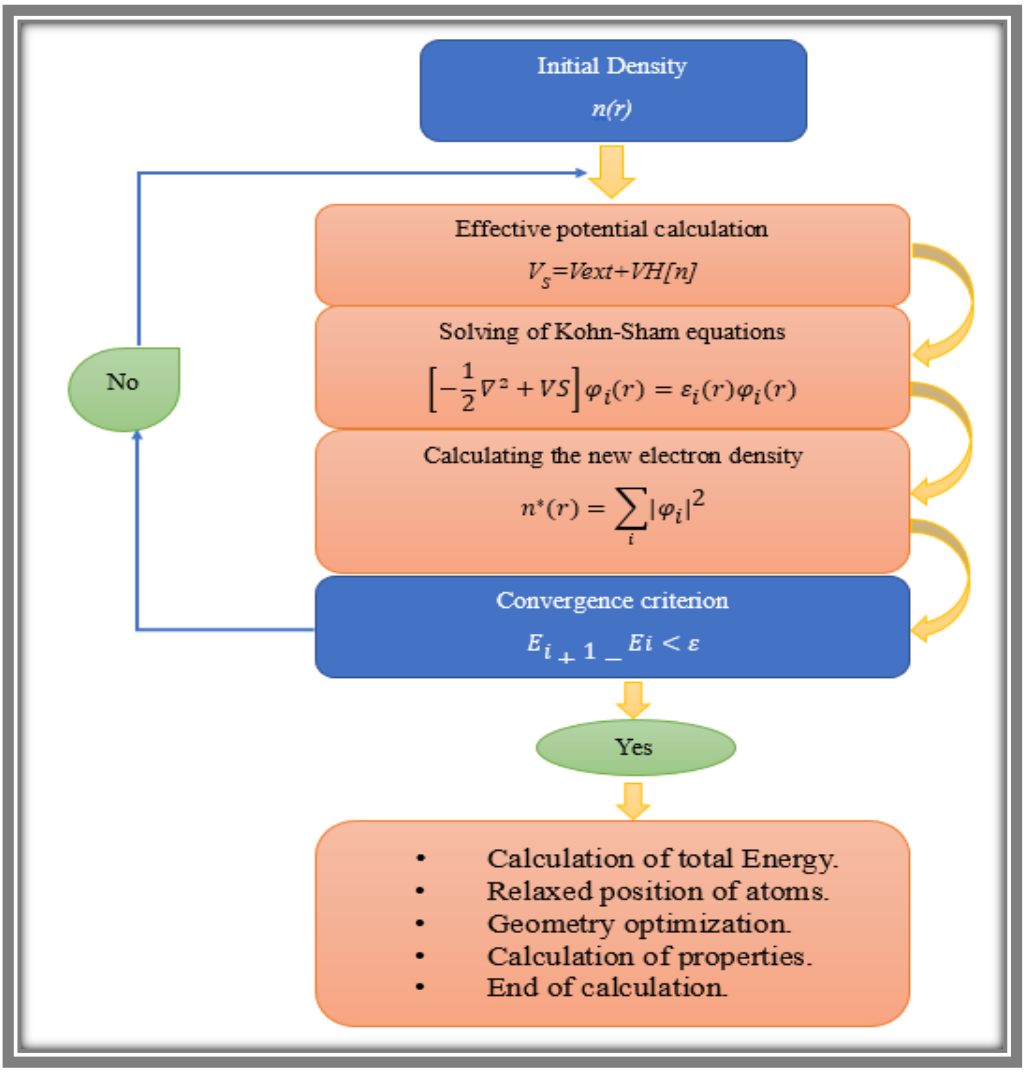

Figure II.3 *Diagram describing the iterative process for solving the Kohn-Sham equations*

II.7 Practical implementations of the DFT

II.7.1 Pseudo potential method

The basic idea behind pseudo potentials is to substitute the true potential resulting from the nuclear charge and core electrons with an effective potential within a core region of radius Rc, as shown schematically in Figure II.5. The effective potential is then subjected to some conditions. The valence orbital eigenvalues must be the same as those found in an all-electron calculation on the atom. It must also maintain the wave functions' and their first derivatives' continuity across the core boundary. Finally, the charge density in the core region should match that of an all-electron density, implying that the pseudo potential must be norm-conserving. At energies corresponding to valence eigenvalues, a pseudo potential that meets these parameters will have the same scattering properties as the ionic core it replaces.

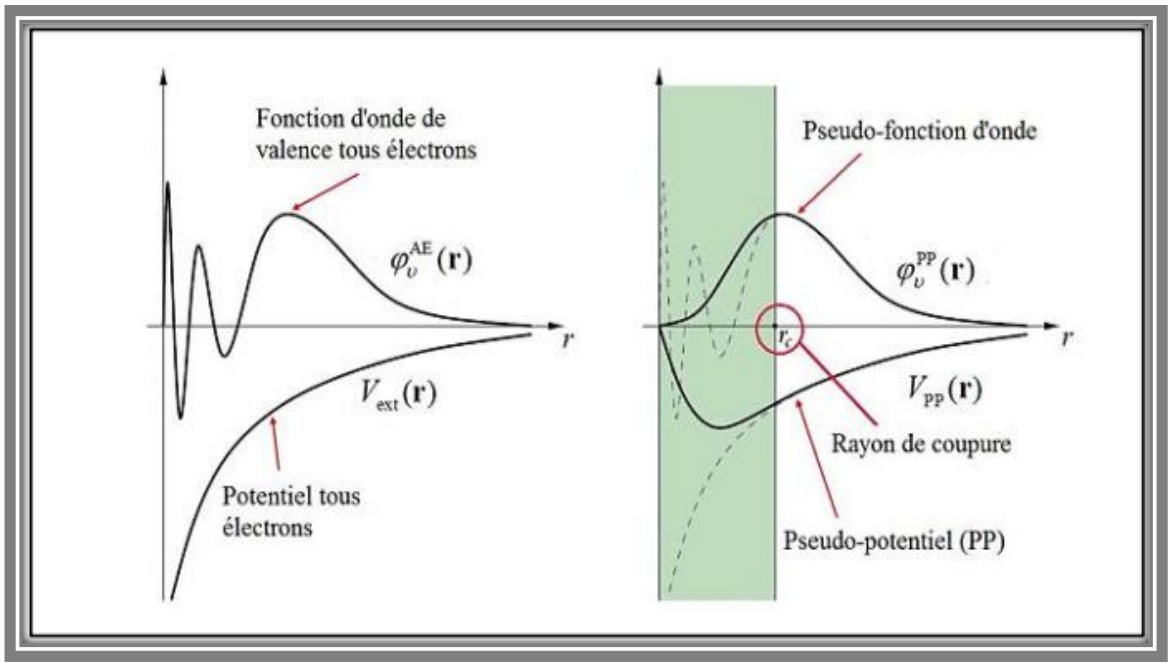

Figure II.4 *Illustration schematizes the potential of all-electron and pseudo-electron and their corresponding wave functions (21).*

II.7.2 Periodic Systems and Bloch theorem

Bloch theorem is a result of the periodicity of the crystalline potential (22), and it uses translational symmetry to demonstrate the system's invariance. The wave function is therefore

expressed as the product of a periodic function, with U owning the periodicity of the lattice and a plane wave.

$$\Psi_j^K\left(\vec{r}\right)=U_j^K\left(\vec{r}\right)e^{i\left(\vec{k},\vec{r}\right)} \quad \text{(II. 35)}$$

and

$$U_j^K\left(\vec{r}\right)=\sum_G \breve{U}\left(\vec{G}\right)e^{i\left(\vec{G},\vec{r}\right)} \quad \text{(II. 36)}$$

Within the first zone Brillouin, the vectors $\vec{k}$ and $\vec{G}$ are specified in reciprocal space. Within a periodic system, Kohn and Sham equations must be solved for a finite number of points K points generated via an appropriate representative sampling of the ZB that permits to faithfully recreate its symmetry.

II.7.3 Sampling of the Brillouin Zone (BZ)

Brillouin-zone sampling is taken into account in total-energy estimates of aperiodic systems with periodic boundary conditions. Although all k-point sampling schemes converge to the exact result in the limit of huge supercells, the energies do not converge at the same rate. It has been demonstrated that using a single sample point at the reciprocal space's origin is particularly wasteful. Monkhorst and Pack provide a computationally efficient k-point sampling approach that is adequate and representative (23).

II.7.4 Plans waves

The plane-wave pseudo potential (PW-PP) approach starts with a three-dimensional periodic super cell to represent the system. As a result, Bloch's theorem which is based on the system's periodicity makes it easier to solve the Kohn-Sham equation, and reduces the unlimited number of one-electron wave functions in the real system to only the number of electrons in the chosen super cell.

$$\Psi_{n,k}\left(\vec{r}\right)=u_{n,k}\left(\vec{r}\right)e^{\left(i\vec{k},\vec{r}\right)} \quad \text{(II. 37)}$$

The super-periodicity cell's is represented by the function $u\left(\vec{r}\right)$. It can have any mathematical shape, but most people opt for a series expansion in terms of a set of basic functions. Plane waves

are employed in the PW-PP technic for this expansion; therefore, each single-electron wave function $\Psi_{n,k}$ is expressed as:

$$\Psi_{n,k}\left(\vec{r}\right)=\sum_{G}C_{n,k}\left(\vec{G}\right)e^{\left(i\left(\vec{k}+\vec{G}\right),\vec{r}\right)} \qquad \text{(II. 38)}$$

The expansion coefficients are denoted by the letter $C_{n,k}\left(\vec{r}\right)J$. The wave vectors $\vec{G}$ are arranged in such a way that the plane waves are proportional to the super-cell. In theory, both the number of **G**-vectors in the sum and the number of **k**'s are unlimited.

II.8 Calculation Code: CASTEP

All of the calculations presented in the manuscript were performed using a digital modeling code called CASTEP (Cambridge Serial Total Energy Package) (24). This code was originally developed in 1988 by Payne et al (25). This is an ab initio computer code and is part of a set of digital simulation software called Materials Studio (MS) and marketed by Dassault Systemes Biovia ©. CASTEP is developed in the Condensed Matter Theory group at the University of Cambridge, UK, it is a program that employs density functional theory (DFT) to simulate the properties of solids, and can predict properties including elastic constants, structural properties, energy band diagrams, electronic state densities, charge densities and optical properties as well as vibrational and thermodynamic properties. This code is used to simulate the total energy by special integration of the points in the first Brillouin zone with a plane wave base for the expansion of the wave functions and the summation in this zone carried out on the vectors of waves produced by the method of Monkhorst and Pack (26).

CASTEP works on Windows and Linux. A graphical interface conforming to Microsoft Windows standards, allows the user to interact with 3D graphic models, configure the calculations and analyze the results through simple dialog boxes familiar to any Windows user (27).

II.9 Elastic properties of the solid

Several fundamental features of the solid state, such as specific heat, thermal expansion, and Debye temperature, are strongly related to the elastic characteristics of solids. The identification of the appropriate elastic constants simplifies the investigation of a material's elastic behavior;

these constants give information on the nature of the solid's chemical bonds, stiffness, elastic anisotropy, and mechanical stability.

II.9.1 Elasticity of isotropic solids

When a medium undergoes only reversible deformations and the forces that cause these deformations are removed, the medium recovers to its original shape. According to Hooke's rule, the deformation is linearly proportional to the applied stress in the field of elasticity; this statement is valid for isotropic materials in the limit of tiny deformations (in an isotropic material, all directions are identical). The stress can be represented as a tensor σ_{ij}, where the index i denotes the force's direction and the index J is the normal to the plane where the force acts.

In linear elasticity theory, there is a linear relation between σ and ε given by the generalized Hooke's law:

$$\sigma_{ij} = C_{ijkl}\varepsilon_{kl} \qquad \text{(II. 39)}$$

Where $i, j, k, l = 1, 2, 3$ and C_{ijkl} is a tensor of order 4 called tensor of elastic rigidity and it defines the elastic constants of the material. The tensor of deformability constants (tensor of supplications) S_{ijkl} can be defined reciprocally by the following relation:

$$\varepsilon_{ij} = S_{ijkl}\sigma_{kl} \qquad \text{(II. 40)}$$

Due to the symmetry of the stress tensor $\left(\sigma_{ij} = \sigma_{ji}\right)$ and the deformation tensor, $\left(\varepsilon_{ij} = \varepsilon_{ji}\right)$ the number of independent components of C_{ijkl} is reduced to 36 (6×6 matrix). In contracted notation of Voigt (transformation of the indices), the matrix expression of the rigidity components is simplified, C_{ijkl} becomes $C_{ij}\left(i, j = 1 \text{ to } 6\right)$. Similarly, for the deformability constants.

Thus, Hooke's law is put in the following matrix form:

$$\underbrace{\begin{pmatrix}\sigma 11\\ \sigma 12\\ \sigma 13\\ \sigma 14\\ \sigma 15\\ \sigma 16\end{pmatrix}}_{Constraints} = \underbrace{\begin{bmatrix}C11 & C12 & C13 & C14 & C15 & C16\\ C21 & C22 & C23 & C24 & C25 & C26\\ C31 & C32 & C33 & C34 & C35 & C36\\ C41 & C42 & C43 & C44 & C45 & C46\\ C51 & C52 & C53 & C54 & C55 & C56\\ C61 & C62 & C63 & C64 & C65 & C66\end{bmatrix}}_{Constants\ of\ elasticity} \underbrace{\begin{pmatrix}\varepsilon 11\\ \varepsilon 12\\ \varepsilon 13\\ \varepsilon 14\\ \varepsilon 15\\ \varepsilon 16\end{pmatrix}}_{Deformation} \qquad \text{(II. 41)}$$

The flexibility matrix $S_{ij} = \left(C_{ij}\right)^{-1}$, has the same number of constants as the inverse of stiffness matrix. The number of independent elastic constants C_{ij} necessary to describe a crystalline solid's elastic behavior is determined by its symmetry. It rises as symmetry is reduced; for example, if the crystal possesses triclinic symmetry, the total number of C_{ij} equals 21. The number of independent elastic constants for each crystalline system is shown in Table II.1.

Table II.2 *The number of elastic constants* C_{ij} *for each crystalline system.*

Crystalline systems	**Number of** C_{ij}
Triclinique	21
Monoclinique	13
Orthorhombique	9
Tétragonal	7-6
Rhomboédrique	7-6
Hexagonal	5
Cubique	3

For an orthorhombic structure (the crystal structure of the herein studied materials) is characterized by nine independent elastic constants C_{11}, C_{12}, C_{13}, C_{22}, C_{32}, C_{33}, C_{44}, C_{55} and C_{66} all other constants are equal to zero. The tensor of the elastic constants is written in this case:

$$Cij = \begin{bmatrix} C_{11} & C_{12} & C_{13} & 0 & 0 & 0 \\ C_{12} & C_{22} & C_{23} & 0 & 0 & 0 \\ C_{13} & C_{23} & C_{33} & 0 & 0 & 0 \\ 0 & 0 & 0 & C_{44} & 0 & 0 \\ 0 & 0 & 0 & 0 & C_{55} & 0 \\ 0 & 0 & 0 & 0 & 0 & C_{66} \end{bmatrix} \quad \text{(II. 42)}$$

II.9.2 Conditions of mechanical stability

The matrix of elastic constants must be positively defined in order for mechanical stability to exist. Mechanical stability of a crystal structure means that the internal energy variation under any minor deformation is positive. This condition can be expressed in terms of C_{ij} elastic constants.

The mechanical stability of an orthorhombic system requires that their independent elastic constants obey the following Born conditions (28).

$$\begin{cases} C_{ii} > 0 \left(i = 1, 4, 5, 6 \right) \\ C_{11}C_{22} > C_{12}^2 \\ C_{11}C_{22}C_{33} + 2C_{13}C_{13}C_{23} - C_{11}C_{23}^2 - C_{22}C_{13}^2 - C_{33}C_{12}^2 < 0 \end{cases} \quad \text{(II. 43)}$$

II.9.3 Polycrystalline elastic moduli

The bulk modulus B and the shear modulus G fully characterize the elastic behavior of an isotropic system. The Young's modulus E and the Poisson's coefficient can be calculated using these two independent elastic moduli.

The Voigt-Reuss-Hill approximation is used to compute these polycrystalline elastic moduli. The highest limit of Voigt corresponds to the average of Hooke's C_{ij} for all possible grain orientations. It is based on the premise that grain deformation is uniform. The Reuss lower limit, like the Voigt limit, averages the inverse relationship S_{ij} and is based on the assumption that stress is homogeneous across each grain. The Hill's average of polycrystalline elastic moduli is used in practice. These modules are defined for an orthorhombic system by the equations in Table II.2,

where the ***V*** and ***R*** indices correspond to Voigt and Reuss, respectively. A practical estimate of true polycrystalline elastic modules is given by the Hill average:

$B_H = (B_V + B_R)/2$ $G_H = (G_V + G_R)/2$

Table II.3 *The physical significance of each elasticity modulus and its equation as a function of Cij in the Voigt and Reuss methods approximations.*

Modules of elasticity	Physical meaning	Equation
Compressibility module	Hydrostatic pressure change resistance	$B_V = \frac{1}{9}\left[C_{11} + C_{22} + C_{33} + 2(C_{12} + C_{13} + C_{23})\right]$ $B_R = \left[S_{11} + S_{22} + S_{33} + 2(S_{12} + S_{13} + S_{23})\right]^{-1}$
Shear modulus	Resistance to the sliding motion of the planes inside the solid	$G_V = (C_{11} + C_{22} + C)_{33} - (C_{12} + C_{13} + C_{23}) + + 3(C_{44} + C_{55} + C_{66})$ $15G_R = 4(S_{11} + S_{22} + S_{33}) - (S_{12} + S_{13} + S_{23}) + + 3(S_{44} + S_{55} + S_{66})$
Young's module	Resistance to uni-axial deformation	$E = \frac{9BG}{3B + G}$
Poisson coefficient	Characterizes the contraction of matter perpendicular to the direction of applied effort.	$\upsilon = \frac{3B - 2G}{2(3B + G)}$
Vickers hardness Chens's model (29)	Defined as the resistance of a material to various types of deformations.	$H_V = 0.1475 \times G$

Where V, R the indices refer respectively to Voigt, Reuss. A practical estimate of true polycrystalline elastic modules is given by the Hill average: $B_H = (B_V + B_R)/2$ and $G_H = (G_V + G_R)/2$

The elastic anisotropy is mechanically expressed as a relationship between the elastic response of a crystalline material and the stress direction. In our research, four distinct technics were used to define it:

Table II.4 *The physical meaning of each anisotropy index and its corresponding equation.*

Indices of anisotropy	Equation	Physical meaning
The universal anisotropy	$A^U = 5\frac{G_V}{G_R} + \frac{B_V}{B_R} - 6$	For an isotropic system A^U=0, while any deviation from zero indicates the degree of anisotropy
Percentage of anisotropy in compressibility	$A_B = \frac{B_V - B_R}{B_V + B_R} \times 100$	0% indicates isotropic behavior, while of all deviation from the extent of elastic anisotropy.
Percentage of shear anisotropy	$A_G = \frac{G_V - G_R}{G_V + G_R} \times 100$	
Coefficients of anisotropies in shear	$A_1 = \frac{4C_{44}}{C_{11} + C_{33} - 2C_{13}}$ $A_2 = \frac{4C_{55}}{C_{22} + C_{33} - 2C_{23}}$ $A_3 = \frac{4C_{66}}{C_{11} + C_{22} - 2C_{12}}$	The degree of shear anisotropy can be identified by the deviation of these coefficients of unity.

Where A1 is the shear anisotropy coefficient for plans (100) between directions (011) and (010), A2 is the shear anisotropy coefficient for plans (010) between directions (101) and (001), and A3 is the shear anisotropy coefficient for plans (001) between directions (110) and (010).

Graphing a three-dimensional surface map of the directional dependency of the elastic modules is another valuable and more direct technic to discover elastic anisotropy. Each point on this surface is identified by a position vector, whose module indicates the value of the elastic quantity measured in the direction specified by the vector's direction cosines in spherical coordinates. For an orthorhombic crystal, the directional dependence of Young's modulus and bulk modulus is given by (30):

$$B = \left[\begin{matrix} S_{11}l_1^4 + S_{22}l_2^4 + S_{33}l_3^4 + \left(2S_{13} + S_{55}\right)l_1^2 l_3^2 + \\ + \left(2S12 + S_{66}\right)l_1^2 l_2^2 + \left(2S_{23} + S_{44}\right)l_2^2 l_3^2 \end{matrix} \right]^{-1} \qquad \text{(II. 44)}$$

$$E=\left[\left(S_{11}+S_{12}+S_{13}\right)l_1^2+\left(S_{12}+S_{22}+S_{23}\right)l_2^2+\left(S_{13}+S_{23}+S_{33}\right)l_3^2\right]^{-1} \quad \text{(II. 45)}$$

Where S_{ij} are the compliance constants of the material, and l_i are direction cosines of direction respectively given in spherical coordinates by:

$$\begin{cases} l1=\cos\left(\varphi\right)\sin\left(\theta\right) \\ l2=\sin\left(\varphi\right)\sin\left(\theta\right) \\ l3=\cos\left(\theta\right) \end{cases} \quad \text{(II. 46)}$$

Isotropic behavior is indicated by a perfect spherical form. Any divergence from sphericity, however, shows some degree of anisotropy.

II.9.4 Debye temperature and elastic wave velocities

The Debye temperature is one of the most critical characteristics that governs the thermodynamic properties of materials. It is the temperature at which the atoms in a solid reach their maximum number of potential modes of vibration. The Debye temperature may be calculated at low temperatures using the average acoustic wave velocities, which are then related to the elastic moduli using the following equations:

$$\theta_D=\frac{h}{K_B}\left[\frac{3n}{4\pi}\left(\frac{\rho N_A}{M}\right)\right]^{1/3}V_M \quad \text{(II. 47)}$$

$$V_M=\left[\frac{1}{3}\left(\frac{2}{V_t^3}+\frac{1}{V_L^3}\right)\right]^{-1/3} \quad \text{(II. 48)}$$

$$V_t=\left(\frac{G}{\rho}\right)^{1/2} \quad \text{(II. 49)}$$

$$V_l=\left(\frac{3B+4G}{3\rho}\right)^{1/2} \quad \text{(II. 50)}$$

Where ***h*** is the Planck constant, K_B is the Boltzmann constant, ***n*** is the number of atoms per molecule, N_A is the Avogadro number, ρ is the density of the material, and ***M*** is the molecular weight. V_M , V_l and V_t are respectively the average, longitudinal and transverse acoustic wave velocities.

II.10 Optical properties

The discipline of physics that deals with illuminating phenomena is known as optics. The various methods in which light interacts with materials in solid state physics, such as absorption, transmission, reflection, diffusion, and emission, are of great interest. The study of solid optical properties has shown to be a valuable tool in our knowledge of material electronic characteristics.

II.10.1 The dielectric function

When a material K is exposed to an electromagnetic wave's oscillating electric field, its dielectric function characterizes its optical response. The electronic transitions between the valence bands and the conduction bands determine this physical quantity, which is heavily influenced by the configuration of the material's energy bands. and it comprises of a real and an imagined element, it is given by (31),

$$\tilde{n} = n + ik \qquad \text{(II. 51)}$$

In reality, the two real parts $\varepsilon_1(\omega)$ and imaginary $\varepsilon_2(\omega)$ of the dielectric function are not independent of each other. Indeed, each can be deduced knowing the other by using the Kramers-Kronig relation (32).

$$\varepsilon_1(\omega) = 1 + \frac{2}{\pi} P \int_0^{\infty} \frac{\omega \varepsilon_2(\omega')}{(\omega')^2 - \omega^2} d\omega' \qquad \text{(II. 52)}$$

$$\varepsilon_2(\omega) = -\frac{2}{\pi} P \int_0^{\infty} \frac{\varepsilon_1(\omega') - 1}{(\omega')^2 - \omega^2} d\omega' \qquad \text{(II. 53)}$$

Where ω is the frequency and ***P*** is the main part of the Cauchy integral.

II.10.2 The refractive index

The refractive index *n* of a material is defined by the ratio of the speed of light in the vacuum *C* to the speed of light in the material ν according to:

$$n = \frac{c}{v} \tag{II. 54}$$

The complex refractive index is a single quantity that can be used to describe the refraction of a medium. It is commonly denoted by the symbol X, which is described by the equation:

$$\tilde{n} = n + ik \tag{II. 55}$$

The real part of $\tilde{n}$ namely n, is the same as the index of refraction at normal incidence. The imaginary part of n namely k is called the extinction coefficient; Both Quantities are related to the dielectric function by the following two relations (33):

$$n(\omega) = \frac{1}{\sqrt{2}}\left[\sqrt{\varepsilon_1^2(\omega) + \varepsilon_2^2(\omega)} + \varepsilon_1(\omega)\right]^{1/2} \tag{II. 56}$$

$$k(\omega) = \frac{1}{\sqrt{2}}\left[\sqrt{\varepsilon_1^2(\omega) + \varepsilon_2^2(\omega)} - \varepsilon_1(\omega)\right]^{1/2} \tag{II. 57}$$

II.10.3 The absorption coefficient

The absorption coefficient $\alpha(\omega)$ shows how much energy the wave loses as it passes through the material. The following relation (34) can be used to characterize it in terms of the extinction coefficient $k(\omega)$:

$$\alpha(\omega) = \frac{4\pi}{\lambda} k(\omega) \tag{II. 58}$$

Where λ represents the wavelength of light in a vacuum.

II.10.4 Reflectivity

The reflection coefficient, often known as reflectivity, is a measure of how well radiation reflects off a surface. This property defines the colors of metals and is commonly denoted by the symbol $R(\omega)$. It is defined as the ratio of reflected intensity to incident intensity on the surface (35). The following relation (33) is used to compute reflectivity from the index of refraction and extinction coefficient:

$$R(\omega) = \frac{n + ik - 1}{n + ik + 1} \qquad \text{(II. 59)}$$

II.11 Conclusion

We present a brief summary of the few concepts and methodologies used in this study in this chapter. An outline of the density functional theory (DFT) as well as the elastic and optical properties of crystalline materials is given special focus. DFT is based on Hohenberg and Kohn's theorem, which states that all physical parameters of an electron gas's ground state are determined solely by its density. Because of Kohn and Sham's formalism, it is possible to use this theorem to compute the total energy of an electron system. The pseudopotential (PP) approach and the plane wave (PP) method are the two most used ways for constructing the wave function and thus the electrical density. The approximation of hybrid functions, the generalized gradient (GGA) approximation, and the local density approximation are three approximations utilized in actual exchange-correlation energy estimates (LDA). In addition, an overview of the CASTEP code is provided.

References

1. **Schrödinger, E.** *Quantisierung als eigenwertproblem.* s.l. : Annalen der physik, 1926. 385(13): p. 437-490.

2. **M, Born, R, J Openheimer.** *Zur Quant en théorie der Molekeln.* s.l. : Ann, Phys,, 1927. 84,457.

3. **Levy, M.** s.l. : Proc Natl. Acad. Sci, 1979. 76,6062.

4. **Sham, W. Kohn and L.J.** s.l. : Phys. Rev., 1965. A 140, 1133,.

5. **Med, Boualleg.** *Mémoire de magister.* Université Guelma : s.n., 2012.

6. **Kohn, P. Hohenberg and W.** s.l. : Phys. Rev, 1964. B, 136, 864.

7. **Hartree, D.R.** *The wave mechanics of an atom with a non-Coulomb central field.* Cambridge University Press : s.n., 1928.

8. **Haddadi, K.** *Thèse de doctorat.* Université Sétif : s.n., 2013.

9. **Thomas, L.** *The effect of the orbital velocity of the electrons in heavy atoms on their stopping of α-particles. in Mathematical Proceedings of the Cambridge Philosophical Society.* Moscou : Cambridge University Press, 1927.

10. **Fermi, E.** *Un metodo statistico per la determinazione di alcune priorieta dell'atome.* Rend. Accad. Naz. Lincei, : s.n., 1927. 6(602-607): p. 32.

11. **Hohenberg, P. and W. Kohn.** *Inhomogeneous electron gas.* s.l. : Physical review, 1964. 136(3B): p. B864.

12. **Kohn, W. and L.J. Sham.** *Self-consistent equations including exchange and correlation effects.* s.l. : Physical review, 1965. 140(4A): p. A1133.

13. **Dirac, P.A.** *Discussion of the infinite distribution of electrons in the theory of the positron.* s.l. : Cambridge University Press, 1934.

14. **Ceperley, D.M. and B. Alder.** *Ground state of the electron gas by a stochastic method.* s.l. : Physical Review Letters, 1980. 45(7): p. 566.

15. **Combelles, C.** *Modélisation ab-initio Appliquée à la Conception de Nouvelles Batteries Li-Ion.* s.l. : Université Montpellier II-Sciences et Techniques du Languedoc, 2009.

16. **Becke, A.D.** *Density-functional exchange-energy approximation with correc asymptotic behavior.* s.l. : Physical Review A, 1988. 38(6): p. 3098-3100.

17. **Perdew, J.P.** *Unified theory of exchange and correlation beyond the local density approximation.* s.l. : Electronic structure of solids' 91, 1991. 11.

18. **Perdew, J.P., K. Burke, and M. Ernzerhof.** *Generalized gradient approximation made simple.* s.l. : Physical review letters, 1996. 77(18): p. 3865.

19. **Hammer, B., L.B. Hansen, and J.K Nørskov.** *Improved adsorption energetics within density-functional theory using revised Perdew-Burke-Ernzerhof functionals.* s.l. : Physical Review B, 1999. 59(11): p. 7413..

20. **Wahl, R., D. Vogtenhuber, and G. Kresse.** *SrTiO 3 and BaTiO 3 revisited using the projector augmented wave method: Performance of hybrid and semilocal functionals.* s.l. : Physical Review B, 2008. 78(10): p. 104116..

21. **Liu, G. Xu, C. Song, Z. Ren, G. Han and Y. Zheng.** *Materials Science and Engineering.* s.l. : Phys.

22. **Kiréev, P.** *La physique des semiconducteurs. 2e édition.* 2éme édition. Moscou : édition Mir, 1975.

23. **Makov, G., R. Shah, and M. Payne.** *Periodic boundary conditions in ab initio calculations. II. Brillouin-zone sampling for aperiodic systems.* s.l. : Physical Review B, 1996. 53(23): p. 15513.

24. **S. Pugh, F. Phil.** s.l. : Mag, 1954. 45 (367), 823.

25. **Payne, M.C., et al.** *Iterative minimization technics for ab initio total-energy calculations: molecular dynamics and conjugate gradients.* s.l. : Reviews of modern physics, 1992. 64(4): p. 1045.

26. **J. J. Wang, F. Y. Meng, X. Q. Ma, M. X. Xu and L. Q. Chen, J. Appl.** s.l. : Phys, 2010. 108.034107.

27. **Monkhorst, H.J. and J.D. Pack.** *Special points for Brillouin-zone integrations.* s.l. : Physical Review B, 1976. 13(12): p. 5188-5192.

28. **Mouhat, F. and F.-X. Coudert.** *Necessary and sufficient elastic stability conditions in various crystal systems.* s.l. : Physical Review B, 2014. 90(22): p. 224104.

29. **Guechi, A., et al.** *Pressure effect on the structural, elastic, electronic and optical properties of the Zintl phase KAsSn, first principles study.* s.l. : Journal of Alloys and Compounds, 2015. 623: p. 219-228.

30. **Nye, J.F.** *Physical properties of crystals: their representation by tensors and matrices.* s.l. : Oxford university press, 1985.

31. **Hosseini, S., T. Movlarooy, and A. Kompany.** *First-principles study of the optical properties of PbTiO 3.* s.l. : The European Physical Journal B-Condensed Matter and Complex Systems, 2005. 46(4): p. 463-469.

32. **Wooten, F.** *Optical Properties of Solids.* New York and London : Academic Press, 1972.

33. **Saha, S., T. Sinha, and A. Mookerjee.** *Structural and optical properties of paraelectric SrTiO3.* s.l. : Journal of Physics: Condensed Matter, 2000. 12(14): p. 3325.

34. **Goubin, F.** *Relation entre fonction diélectrique et propriétés optiques: application à la recherche d'absorbeurs UV inorganiques de deuxième génération.* s.l. : Université de Nantes, 2003.

35. **Dupeux, M.** *AIDE-MEMOIRE SCIENCE DES MATERIAUX.* s.l. : Dunod, 2004.

RESULTS AND DISCUSSION

III.1 Introduction

In this chapter, we will present the results for the optimized structural parameters and the predicted elastic, optical and electronic properties of the orthorhombic Zintl compounds A_2CuAs (A=*Na*, *K*).

III.1.1 Calculation details

All calculations conducted in the present work were performed using the CASTEP code based on the pseudo-potential and plane waves schemes (PP-PW) of DFT theory. We make use of Generalized Gradient Approximation (GGA) as parameterized by Perdew-Burk-Ernzerhof "PBE". The electron-ionic interactions were treated using on-the-fly generated OFTG Norm conserving pseudo-potentials (1). For an accurate prediction of the subsequent key physical properties, scaler relativistic effect has been considered in the generation of the pseudo potential using the technic proposed by Koelling Hamon (2). Valence states were modelled by ($3s^2 3p^6 4s^1$) for *K*, ($2s^2 2p^6 3s^1$) for *Na*, ($3d^{10} 4s^1$) for *Cu*, ($3d^{10} 4s^2 4p^3$) for *As*. In a DFT calculation, the physical properties of a system are functional of the electron density of the ground state. This density is the one that minimizes the total energy of the system. It is therefore required to express this energy with the greatest possible precision. In order to ensure convergence of the computed structures and energies, the parameters that affect the calculation accuracy were selected after performing careful convergence tests. The self-consistent loop was iterated until the total energy difference of the system between the consecutive iterating steps becomes less than 10^{-6} eV/atom. First, the Cutoff energy (E_{cut}) convergence study has been performed, then convergence with respect to Brillouin zone sampling has been conducted, the results are reported in the next section.

III.2 Convergence study

Before moving to the computation of the various ground state physical properties, it is required to optimize the calculation settings. That is to say, it is a matter of optimizing the size of the plane wave basis set on which the Kohn and Sham orbitals are defined, as well as the number of points k (Nkpt) used for integration in the irreducible Brillouin zone.

III.2.1 Choice of the size of the plane wave basis set

The Kohn-Sham pseudo orbitals are decomposed on a plane wave basis set. Nevertheless, this decomposition is only correct if the basis set is infinite. Unfortunately, this is numerically impossible. As a result, the basis set is truncated to a finite size. The value of the kinetic energy of

the plane wave with the greatest frequency determines the size of the basis set on which the electronic wave function is projected. This energy is known as cutoff energy Ecut. When the total energy as a function of the cutoff energy reaches a standing value, we may claim that the basis size is sufficient; hence, the total energy has converged.

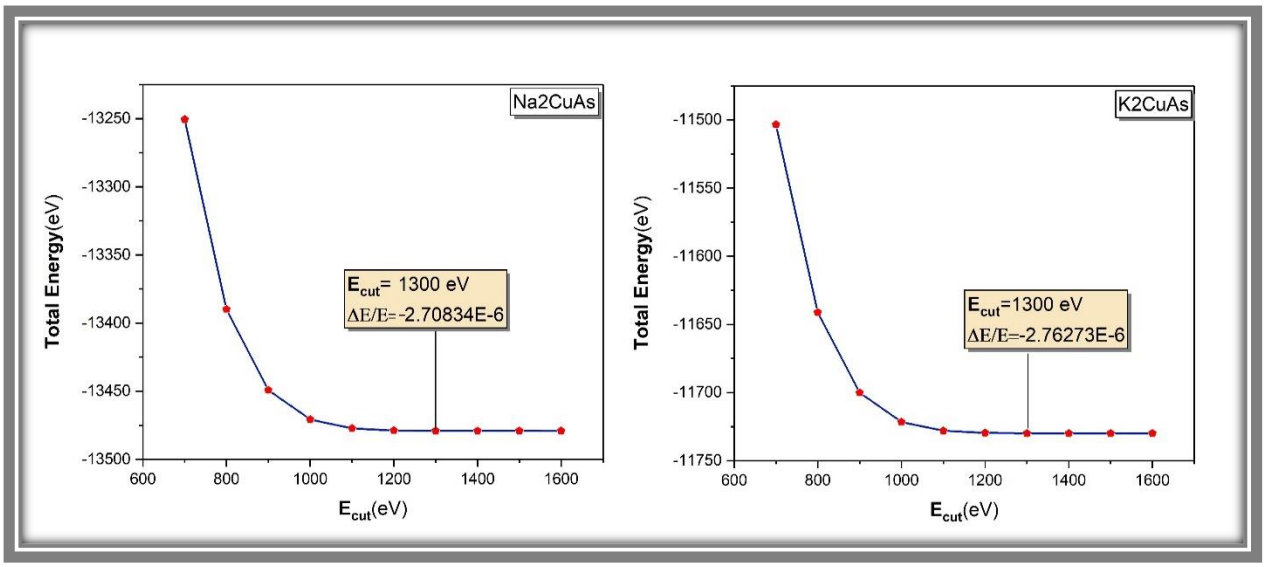

Figure III.1 *Convergence of the total energy as a function of E_{cut} for compounds A_2CuAs (A=K, Na).*

Table III.1 *Convergence of total energy as a function of Ecut for K_2CuAs with the relative variation of energy.*

K_2CuAs		
E_{cut} *(eV)*	**Total Energy (eV)**	$\Delta E/E_F$
700	-11503.37354764	-0.01932
800	-11641.21352785	-0.00756
900	-11700.08990787	-0.00254
1000	-11721.60140286	-7.10681E-4
1100	-11728.0722421	-1.59029E-4
1200	-11729.6368912	-2.56397E-5
1300	-11729.90523331	-2.76304E-6
1400	-11729.93068352	-5.9336E-7
1500	-11729.93415716	-2.97226E-7
1600	-11729.9376436	0

As can be seen from **Figure III.1, t**he converged total energies for K_2CuAs and Na_2CuAs are obtained at a cut-off energy E_{cut} of 1300 eV. **Table III.1** shows the relative error of the total energy of K_2CuAs as a function of E_{cut} which can be considered as an indication of the accuracy of our calculations.

III.2.2 Brillouin Zone (ZB) Sampling

It is necessary to integrate on the k points in the Brillouin zone in order to obtain parameters such as total energy, charge density, and so on. To do so, the calculation must be conducted on a finite number of relevant k points. The integral over the first ZB is approximated by a discrete (finite) sum over a particular set of k points using the conventional Monkhorst and Pack approach (3).

Having optimized the basis set size, the cutoff energy it is set at its optimal value and the number of k points is varied. The total energy is determined for each of these values. When the total energy hits a stationary value as function of the k point number, it is said to be converged with regard to the number of points k.

In this work a good convergence is reached at a sampling grid of (7x7x7) which corresponds to 64 points k in the irreducible zone of Brillouin. Indeed, the relative variation of the total energy $\Delta E/E_F$ is in the order of 10^{-8} for Na_2CuAs and 10^{-9} for K_2CuAs; see **Figure III-2**.

Table III.2 *Convergence total energy functional of k points, for compounds (Ecut=1300 eV).*

Na_2CuAs		
K-points	***Total Energy (eV)***	**ΔE/E**
2 2 2	-1.34792E+04	1.91379E-05
3 3 3	-1.34789E+04	-4.86981E-06
4 4 4	-1.34790E+04	1.20851E-06
5 5 5	-1.34790E+04	-4.73386E-07
6 6 6	-1.34790E+04	1.64166E-07
7 7 7	-1.34790E+04	-7.65703E-08
8 8 8	-1.34790E+04	2.87425E-08
9 9 9	-1.34790E+04	-1.49366E-08
10 10 10	-1.34790E+04	6.23563E-09
11 11 11	-1.34790E+04	-4.07152E-09
12 12 12	-1.34790E+04	0.00000E+00

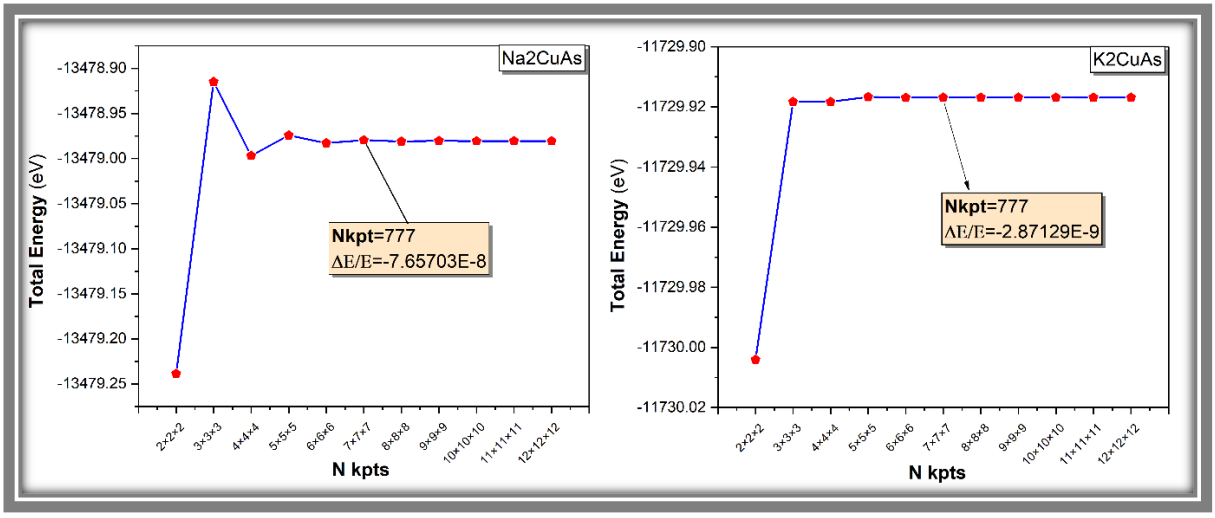

Figure III.2 *Convergence of the total energy as a function of Nkpt for compounds (Na_2CuAs and K_2CuAs).*

III.3 Structural properties

To establish the various proprieties of the ground state, it is necessary to optimize firstly the equilibrium geometry of the system under consideration. This enables us to produce a relaxed structure that has the lowest overall energy. This is accomplished by neutralizing Hellmann-Feynman's forces exerted on the solid's atoms (4; 5).

We start by checking whether the chosen calculation parameters can reproduce accurately the observed experimental ground state geometry. To guarantee strict optimizations, the bulk structures from Refs (6; 7) were used. The Low memory-Broyden-Fletcher-Goldfarb-Shanno (LBFGS) algorithm was employed to minimize total energy in a self-consistent manner (8; 9). Both the lattice parameters and the atomic coordinates were fully relaxed while adhering to the convergence requirements listed below:

- Tolerance in energy: 5.0×10^{-6} eV/atom.
- Max force: 0.005 eV/Å.
- Max stress: 0.01 GPa.
- Max displacement: 5.0×10^{-4} Å.

Table III-3 gives a comparison between the calculated lattice parameters and the atomic positions and those which were determined experimentally by Essenmain (6; 7).

Table III.3 *calculated (Cal) and Experimental (Exp) structural parameters: cell parameters (a, b and c), volume (V), and density (ρ) for A_2CuAs (A=Na, K).*

System	Na_2CuAs			K_2CuAs		
Chemical name	Copper Sodium Arsenide			Copper potassium arsenide		
Space group, Z	Cmcm (No.63), 4 Orthorhombic			Cmcm (No.63), 4 Orthorhombic		
Symmetry						
	Cal	**Exp** (6)	**d(%)**	**Cal**	**Exp** (6)	**d(%)**
Unit cell parameters (Å)	a= 8.9489	a= 8.86	+0.89%	a= 10.1385	a= 10.02	+1.06%
	b= 7.2147	b= 7.22	-0.07%	b= 7.6338	b= 7.56	+0.91%
	c= 5.3629	c= 5.34	+0.37%	c= 5.9430	c= 5.89	+1.04%
a/c	1.668	1.659	+0.53%	1.705	1.701	+0.28%
b/c	1.345	1.352	-0.51%	1.284	1.283	+0.07%
Cell volume ($Å^3$)	346.256	341.6	+1.34%	459.968	446.2	+2.99%
Density (g/cm^3)	3.5382	3,5865	-1.34%	3.1287	3,225	-2.98%

Table III.4 *calculated (Cal) and Experimental (Exp) atomic coordinates (x, y, z) (for A_2CuAs (A=Na, K), and Wyckoff position (P.W).*

	Atoms	**P. W**	**X**		**Y**		**Z**	
			Cal	**Exp** (6)	**Cal**	**Exp** (6)	**Cal**	**Exp**
Na_2CuAs	Na	8g	0.3249	0.3262	0.3532	0.3559	0.25	0.25
	Cu	4b	0	0	0.5	0.5	0	0
	As	4c	0	0	0.2315	0.2343	0.2	0.25
K_2CuAs	K	8g	0.3306	0.331	0.3513	0.354	0.25	0.25
	Cu	4b	0	0	0.5	0.5	0	0
	As	4c	0	0	0.2597	0.261	0.25	0.25

As shown in **Tables III.3** and **III.4,** the resulting equilibrium geometry, including unit cell lattice parameters, atomic coordinates, cell volume and density, are in excellent agreement with their experimental counterparts. The good agreement between our calculated results and the available experimental data illustrates the robustness of the computational methodology used here and gives confidence on the subsequent computed electronic, elastic, and optical properties given in the next sections. Besides, the estimated cell volume and lattice parameters rise as one move

down the periodic table from *K* to *Na*. this is probably due to the rising atomic radii of the alkali-metal atoms.

III.4 Elastic Properties

The determination of the related elastic constants (stiffness tensor) simplifies the investigation of a material's elastic behavior. The anisotropy of interatomic bonding, structural stability, mechanical, vibrational, and thermodynamic characteristics may then be accessible using only the elastic constants, which can be found quickly using ab initio calculations.

In this section, the whole collection of elastic stiffness constants estimated for the Zintl phases under consideration will be used to study their mechanical behavior. To the best of our knowledge, there are no experimental or theoretical data that can be compared to our findings.

III.4.1 Elastic stiffness constants

The static strain technic (10) is used to compute the nine elastic constants for the considered orthorhombic crystal structures: C_{11}, C_{22}, C_{33}, C_{44}, C_{55}, C_{66}, C_{12}, C_{13}, C_{23}. The resulting stress is computed by applying a symmetric unique strain and allowing atomic coordinates to be relaxed. This was done using the following convergence criteria:

- Energy tolerance: 10^{-6} eV/atom
- Maximum forces: 0,002 eV/Å.
- Maximum displacement: 1.0×10^{-4} Å.

The three constants: $\mathcal{C}_{11}$, $\mathcal{C}_{22}$ and $\mathcal{C}_{33}$: represent the uniaxial compressive strength along the principal directions *[100] [010]* and *[001]*, respectively. And the six other constants: $\mathcal{C}_{44}$, $\mathcal{C}_{55}$, $\mathcal{C}_{66}$, $\mathcal{C}_{12}$, $\mathcal{C}_{13}$ and $\mathcal{C}_{23}$: are a measure of the resistance to shear stresses.

Table III.5 gives the elastic constants for Na_2CuAs and K_2CuAs in orthorhombic structure calculated in the GGA-PBE approximation. As can be seen from the data, the three constants C_{11}, C_{22} and C_{33} are greater than the other elastic constants; this clearly shows that the considered materials resist uniaxial compression better than shear strain. In addition, the low values of C_{44}, C_{55}, C_{66}, C_{12}, C_{13} and C_{23} indicate that the mechanical stability of these materials is mainly limited by their low shear strengths.

Table III.5 *Calculated elastic stiffness coefficients (C_{ij}, in GPa) of the A_2CuAs (A=Na, K) compounds.*

	C_{11} (GPa)	**C_{22}** (GPa)	**C_{33}** (GPa)	**C_{44}** (GPa)	**C_{55}** (GPa)	**C_{66}** (GPa)	**C_{12}** (GPa)	**C_{13}** (GPa)	**C_{23}** (GPa)
Na2CuAs	65.72	59.44	55.92	33.85	13.17	9.21	6.13	5.24	28.23
K2CuAs	45.95	39.88	30.82	20.97	07.36	07.40	08.88	07.44	20.89

III.4.2 Mechanical stability

In order to remain mechanically stable, the strain energy of a crystal must be positive. This shows that the entire collection of elastic constants C_{ij} for an orthorhombic crystal must meet the following established stability conditions (11; 12).

$$\begin{cases} C_{ii} > 0 \left(i = 1,4,5,6 \right) \\ C_{11}C_{22} > C_{12}^2 \\ C_{11}C_{22}C_{33} + 2C_{13}C_{13}C_{23} - C_{11}C_{23}^2 - C_{22}C_{13}^2 - C_{33}C_{12}^2 < 0 \end{cases}$$

The estimated elastic stiffness constants reveal that the aforementioned conditions are met, indicating that the compounds under consideration are mechanically stable.

III.4.3 Polycrystalline elastic moduli

Polycrystalline elastic moduli like as Young's modulus, shear modulus, and Poisson's coefficient can be accurately estimated using the latter elastic constants. **Table III.6** summarizes the findings obtained using the Voigt-Reuss-Hill approximation for *K_2CuAs* and *Na_2CuAs*. The lower and higher boundaries of **B** and **G** are given by the Voigt (13) (denoted **V** in index) and Reuss (14) (denoted **R**) moduli, respectively, while the Hill (15) (denoted **H**) moduli offer the mean between the two limits (see chapter II for more details).

In fact, both *K_2CuAs* and *Na_2CuAs* have low bulk modulus (**B**), implying that these materials are soft and easily compressible. The lower **G** values suggest a reduced capacity to tolerate shear strain, showing that the shear modulus **G** is the parameter limiting mechanical stability of these materials. Furthermore, as shown in **Table III.6**, the Young's moduli **E** of the tow materials are

rather low. This demonstrates that these materials have a limited stiffness. The aforementioned results suggest a weak hardness.

Pugh's criteria (B/G) (17) of polycrystalline phases might be used to predict brittle (B/G<1.75) and ductile (B/G>1.75) behavior, according to Pugh's criteria. *Na_2CuAs* must be brittle and *K_2CuAs* must be a ductile material.

Table III.6 *Modules of elasticities calculated by GGA-PBE for polar compounds A_2CuAs (A= Na, K).*

	B_R (GPa)	B_V (GPa)	B (GPa)	G_R (GPa)	G_V (GPa)	G (GPa)	B/G	E	γ
K_2CuAs	21.23	20.80	21.02	09.75	12.44	11.10	1.894	28.31	0.275
Na_2CuAs	28.65	28.92	28.78	15.97	20.68	18.32	1.483	45.35	0.237

The Poisson's ratio governs several phenomena related to the material's elastic behavior. The most basic is that when a material with a negative Poisson's ratio is stretched, it becomes fatter in cross section and when compressed, it becomes thinner. As Poisson's ratio approaches 0.5, the material, as rubber-like materials, easily endures shear deformations but resists volumetric deformation and becomes incompressible (18). Brittle covalent materials have a typical value (γ) of 0.1, ductile metallic materials have a value of 0.33, and ionic materials have a value of 0.25.

Table III.6 shows that the Poisson's ratio of *Na_2CuAs* and *K_2CuAs* is around 0.25. This clearly suggest that a significant ionic bonding character must be assumed.

III.4.4 Elastic anisotropy

Many crystals with poor symmetry have varying extend of elastic anisotropy. As a result, investigating anisotropic behavior in crystal physics and engineering research is critical. The elastic behavior of *Na_2CuAs* and *K_2CuAs* is the focus of this study. There were three technics employed.

1. The so-called universal elastic anisotropy index A^U. Isotropic elastic behavior is indicated by a value of zero. While the any deviation from 0 shows the extend of the elastic anisotropy in both shear and compressibility. In this study, the computed universal anisotropic indexes (A^U) for both materials are larger than zero. High anisotropic mechanical characteristics are shown by the substantial divergence from zero.

2. We estimated the percent anisotropy in compressibility (A_B) and shear (A_G) to understand the origin of this anisotropy. A value of 0% represents a perfect isotropic medium, whereas any deviation from this value reveals the extend of the anisotropic elastic behavior. **Table III.7** shows the obtained results. For the materials addressed here, the percent anisotropy in shear is larger than the percent anisotropy in compressibility. That is to say, in this situation, elastic anisotropy is mostly due to shear anisotropy.
3. We estimated the so-called shear anisotropic factors to obtain further insight into the shear anisotropy of our compounds (see Chapter II). Further examination of the gathered data reveals that all three components differ from one another. The Shear anisotropic component in the primary (001) plane, on the other hand, is the one that deviates the most from unity. That is, among the major plans, the (001) shear plans are most likely to be the cleavage plans.

The research stated above are insufficient to properly characterize the anisotropy of a crystal's elastic behavior. A 3D surface plot of the directional dependence of different elastic moduli such as the Young's modulus and the bulk modulus, which are also the two most commonly used parameters for the description of the elastic behavior of polycrystalline materials, is another useful and more convenient way to quantify elastic anisotropy. The distance between a point on the surface and the origin of the coordinates system in this illustration represents the magnitude of the elastic moduli in a given direction. A perfect isotropic media, in other words, will have a perfect spherical surface. Any deviation from sphericity, on the other hand, shows the presence of anisotropy in the elastic modulus under consideration.

The **equations II.44** and **II.45** can be used to describe the directional dependence of Bulk and Yong's moduli (see chapter II). **Figures III.3** and **III.4**, exhibit the acquired findings. According to the 3D surface plot of the Young's modulus, both materials are large anisotropic. Meanwhile, in accordance with the results of the universal anisotropic index, *Copper Sodium Arsenide* has the greatest degree of elastic anisotropy. As seen in cross sections of the 3D surface plots of Young's modulus in **Figure III.3, t**he highest value of the Young's modulus is achieved when the stress is applied along the bisectors of the (bc) plan, while the smallest value is achieved when the stress is applied in the bisectors of the (ab) plan. As can be seen in **Figure III.4, t**he bulk modulus anisotropy is less significant. Furthermore, the b axis is the most incompressible. This result agrees well with the observed tendency of the elastic stiffness constants.

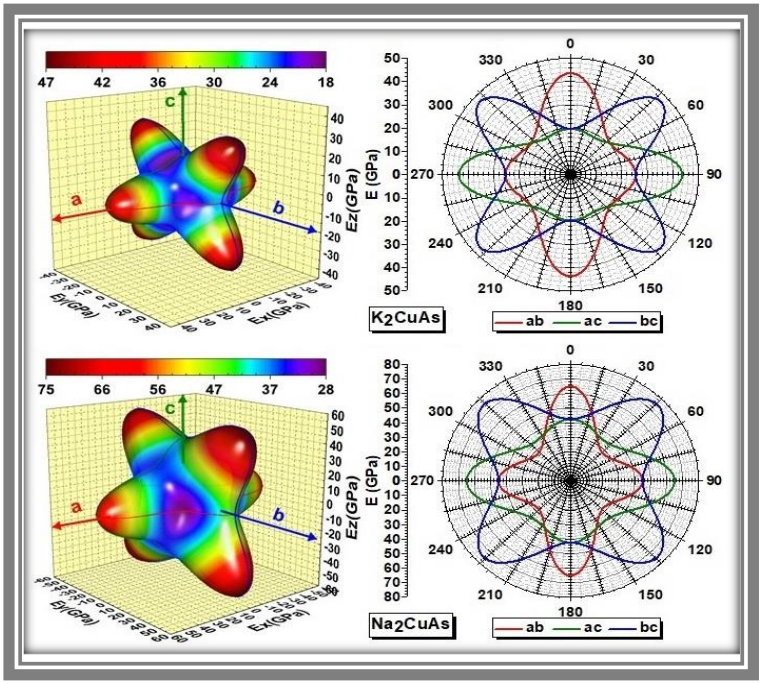

Figure III.3 *Anisotropy of Young's modulus for (Na_2CuAs and K_2CuAs) compounds.*

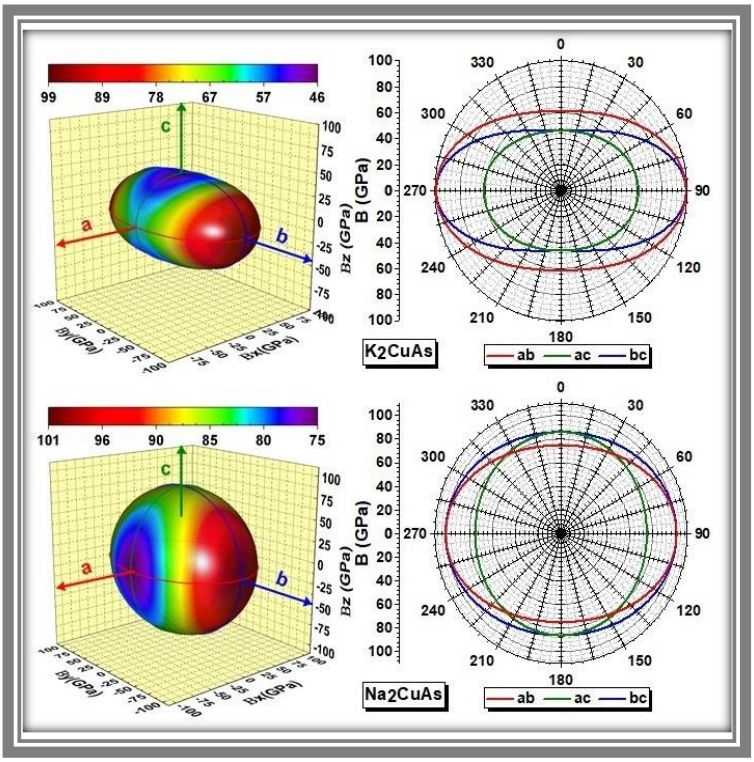

Figure III.4 *Anisotropy of bulk modulus for (Na_2CuAs and K_2CuAs) compounds.*

Table III.7 *Calculated anisotropic indexes for the A_2CuAs (A=Na, K) compounds.*

System	A^U	A_G (%)	A_B (%)	A_1	A_2	A_3
Na_2CuAs	1.484	12.851	1.023	1.218	0.894	0.326
K_2CuAs	1.359	12.122	0.468	1.355	1.017	0.434

III.4.5 Debye temperature

The Debye temperature Θ_D is linked to a number of solid-state phenomena, including lattice vibration, thermal conductivity, melting temperature, specific heat, and so on. It also represents the chemical bonding strength in crystalline materials. The Debye temperature of *Na_2CuAs* and *K_2CuAs* compounds may be calculated using the **equations (II.47,48,49,50)** in Chapter II, which include the average sound velocity V_m, longitudinal propagation velocities V_l, and transverse V_t.

Table III.8 shows the findings that were achieved. Both materials have a low Debye temperature, as seen in this table. The estimated tendency for our compounds is Θ_D(*Na_2CuAs*)>Θ_D(*K_2CuAs*). The low Debye temperature of the materials examined here is owing mostly to their low stiffness and density. Low thermal conductivity can be expected since lattice vibration is mostly caused by acoustic modes at low temperatures, and the obtained average sound velocities are very low.

Table III.8 *Calculated longitudinal acoustic velocities V_l (m/s), shear acoustic velocities V_t(m/s), average acoustic velocities V_m(m/s) and elastic Debye temperatures Θ_D (K) of the A_2CuAs (A=Na, K) compounds.*

	V_l (m/s)	V_t (m/s)	V_m (m/s)	Θ_D (K)
Na_2CuAs	3877.85	2275.47	2522.5301	269.9127
K_2CuAs	3383.61	1883.56	2097.4891	199.3576

III.5 Electronic properties

The study of the electronic properties is crucial because it allows us to analyze and comprehend the nature of the connections that develop between the various constituents of any substance. Electronic band structure, total and orbital projected density states are features that are commonly used to characterize the solid-state electronic structure.

In this study, the electronic properties were investigated using the GGA-PBE approximation with a denser non-shifted k points sampling grid of (16*16*16), which gives 576 with a maximum sampling step of 0.001 $Å^{-1}$.

III.5.1 Structure of the energy bands

The eigenvalues associated with conduction and valence bands in certain directions in the Brillouin zone of a crystal structure are revealed by the solid-state electron band structure. The band gap is one of the most essential reasons for estimating the electronic band structure (the energy gap). That is, the difference between the highest allowable valence band energy and the lowest permissible conduction band energy in the Kohn-Sham method. The predicted electronic band structure helps us to identify the chemical type (metal, insulator, or semiconductor) and provides useful insights into the possible uses for optical device applications.

Figure III.5 Show the Brillouin zone of a representative unit cell of the herein considered materials, along with the corresponding principal directions between the high symmetry points namely, Z(0,0,1/2), T (-1/2,1/2,1/2), Y(-1/2,1/2,0), G(0,0,0), S(0,1/2,0), R(0,1/2,1/2), Γ(0,0,1/2).

Along the high symmetry directions, **Figure III.6** shows the matching electronic band structure derived using the GGA-PBE approximation.

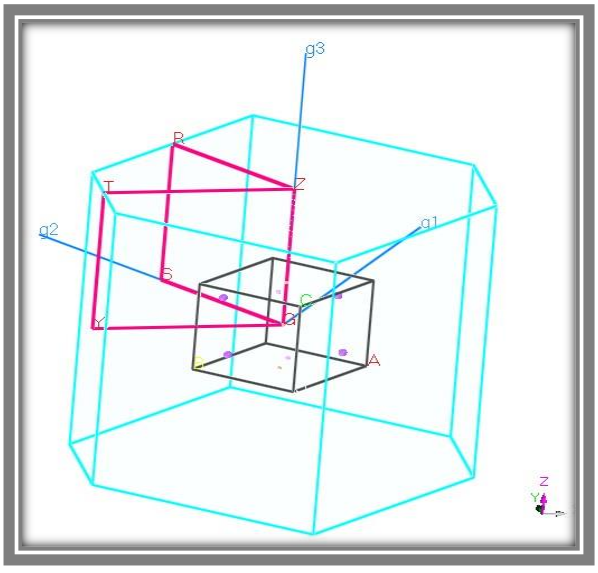

Figure III.5 *First Brillouin zone for the orthorhombic lattice (cmcm) and the points of high symmetry. (g1, g2 and g3 are the vectors of the reciprocal lattice).*

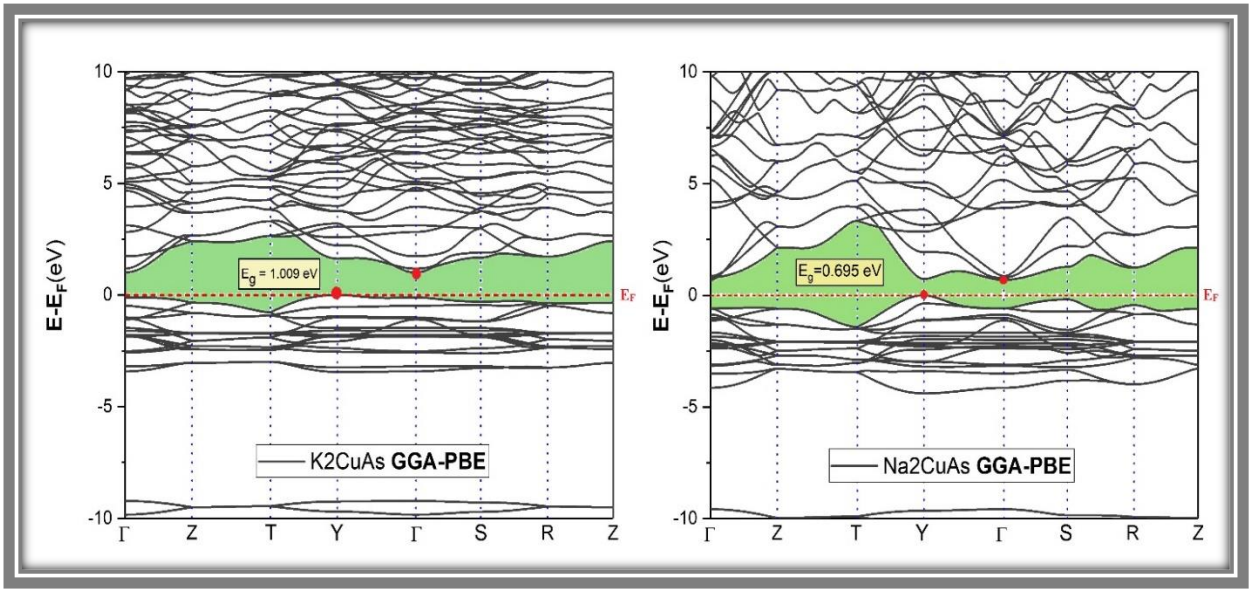

Figure III.6 *Energy band structures of Na_2CuAs and K_2CuAs calculated by GGA-PBE. The Fermi level is set at 0 eV and marked by the dashed red horizontal line*

Using typical GGA-PBE calculations, the calculated band diagrams of the considered materials have many similarities (see **Figure III.6**). Likewise, the highest valence band (VB) at Y and the minimum of the conduction band (CB) at Γ demonstrates that both materials are narrow indirect band gap semiconductors. The computed GGA-PBE band gaps for *Na_2CuAs* and *K_2CuAs* are 0.695 eV and 1.009 eV, respectively.

Above the Fermi level, the minimum of the conduction band at the Γ point is dominated by many folded bands of which, some are very dispersive suggesting low electronic effective mass and excellent mobility. Meanwhile, the non-dispersive band near the valance band maximum show signs of high hole effective mass. The flat almost non dispersed bands along the Z-T, R-Z directions (perpendicular to c*) and the degenerate dispersed bands along the Γ-Z, S-R, T-Y directions (parallel to c) are other important features shared by the band diagrams of the considered materials.

III.5.2 Density of states

The density of states (DOS) is a crucial physical feature for comprehending a material's electronic states and their impact on its physical properties. The majority of electronic transport properties are defined by knowing the density of states. It also enables researchers to determine

the type of chemical bonding in a material, and hence the charge transfer between orbitals and atoms.

The existence of tow valleys in the valence region designated by BV1 and BV2 may be shown clearly in **Figure III.7**. The first valley (BV1) lies slightly below the Fermi level, with a range of -4.5eV to 0eV for Na_2CuAs and 4eV to 0eV for K_2CuAs. It is formed mostly by an admixture of *As*-4p orbitals and *Cu*-3d orbitals, with a minor contribution from a mixing of *Na*-3s / *K*-4s, *Na*-2p / *K*-3p, *Cu*-3p, *Cu*-4s. The significant hybridation between the *Cu*-3d and *As*-3p indicates covalent *As*-*Cu* interaction. The second valley (BV2), which spans approximately from -9.5eV to -10.5eV, is dominated by the confined As-4s states, with modest contributions from *Cu*-4s, *Cu*-3p, *Na*-3s / *K*-4s, and *Na*-2p / *K*-3p.

The conduction band stem primarily from *Na*-3s, *Na*-2p and *K*-4s, *K*-3p with a minor contribution from both *Cu*-4s, *Cu*-3p, *As*-4p, which is compatible with the assumption that the alkali metal atom donates its valance electron to form the neighboring poly-anionic $[CuAs]^{-1}$.

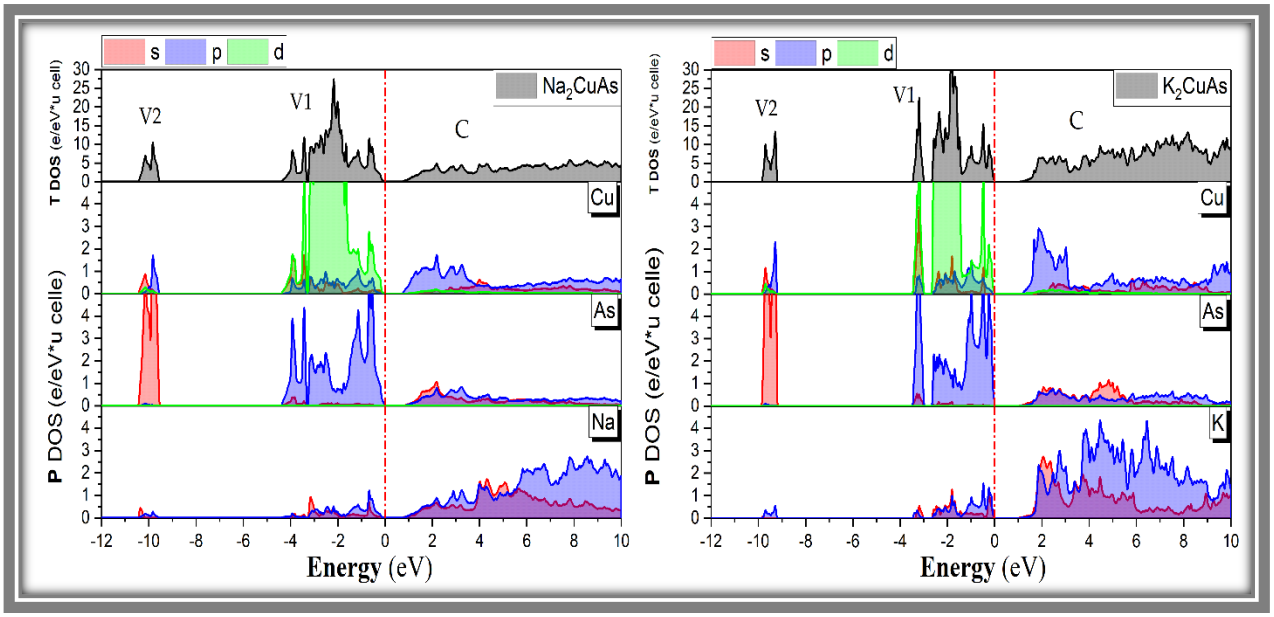

Figure III.7 *Total and partial density of states for K_2CuAs and Na_2CuAs compounds.*

The charge density distribution is a crucial feature of solids that accurately describes their chemical bonding character. The electronic charge distribution between the atoms creates the chemical bonding. The charge transfer between the cations and anions may be connected to a material's ionic nature. Mullikan population analysis was used to obtain further insight into the

charge transfer and chemical bonding image of the materials under consideration (see **Table III.9**). It was found that *Na* transfers +1.32*e* (+0.66*e*×2) to the polyanionic unit in Na_2CuAs, and +1.48*e* (+0.74*e* ×2) is transferred from *K* in K_2CuAs. Our findings demonstrate that Na_2CuAs has an average charge of -0.63*e* per *Cu* and -0.70*e* per *As*, and K_2CuAs has an average charge of -0.65*e* per *Cu* and -0.82*e* per *As*. Therefore, the formal charges of the investigated compounds are $(Na^{+0.66})_2\ Cu^{-0.63}\ As^{-0.70}$ and $(K^{+0.74})_2\ Cu^{-0.65}\ As^{-0.82}$, respectively. We estimated the Mullikan bond populations to investigate charge transfers in these compounds in a more straightforward manner. **Table III.10** summarizes the results collected. There is a clear evidence for a noticeable covalent interaction in the *Cu-As* and *Cu-Cu* contacts along the zigzag chains for both materials, which can be clearly seen in the large positive Mullikan population (MP). Furthermore, *K/Na-Cu* interactions are antibonding by evidence of the negative MP and the *K/Na-As* has a pure ionic nature marked by its very low MP.

In EDD pictures (**Figure III.9**), red regions correspond to an increase in electron density ($\Delta\rho>0$), which gives evidence for a charge density accumulation, whilst blue regions correspond to a depletion in the valence electron density ($\Delta\rho<0$). Overall, the Cu states, and to a lesser degree, the *As* states orientated along the *Cu-As* bond axis, show a distinct depletion at the corresponding atomic sites. Meanwhile, it is evident that there is an accumulation of the charge density at the middle distance of the *Cu-As* thereby corresponding to their covalent bond interaction in both compounds.

Table III.9 *Calculated atomic effective charges fort the A_2CuAs (A=Na, K) compounds.*

Atom	Na_2CuAs	K_2CuAs
A	+0.66	+0.74
Cu	-0.63	-0.65
As	-0.70	-0.82

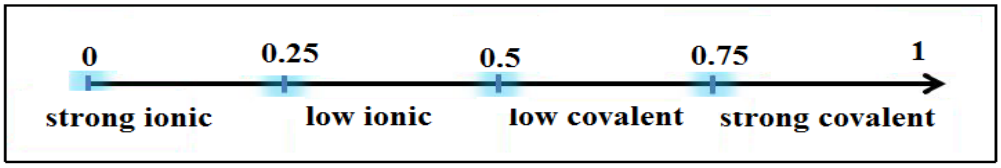

Figure III.8 *Classification of the nature of the bonds according to Mullikan population analysis.*

Table III.10 *Inter-atomic distances (Å) for the A_2CuAs (A=Na, K)*

Band		Distance			M. P
		Cal	Exp (6)	d (%)	
Na_2CuAs	Cu-As	2.3558	2.337	+0.79%	+0.70
	Cu-Cu	2.6815	2.670	+0.42%	+0.60
	Na- As	3.0378	3.020	+0.58%	+0.01
	Na-Cu	3.3727	3.279	+2.77%	-0.21
K_2CuAs	Cu-As	2.3601	2.333	+1.14%	+0.89
	Cu-Cu	2.9715	2.945	+0.89%	+0.36
	K-As	3.5352	3.504	+0.88%	+0.08
	K-Cu	3.5143	3.491	+0.66%	-0.28

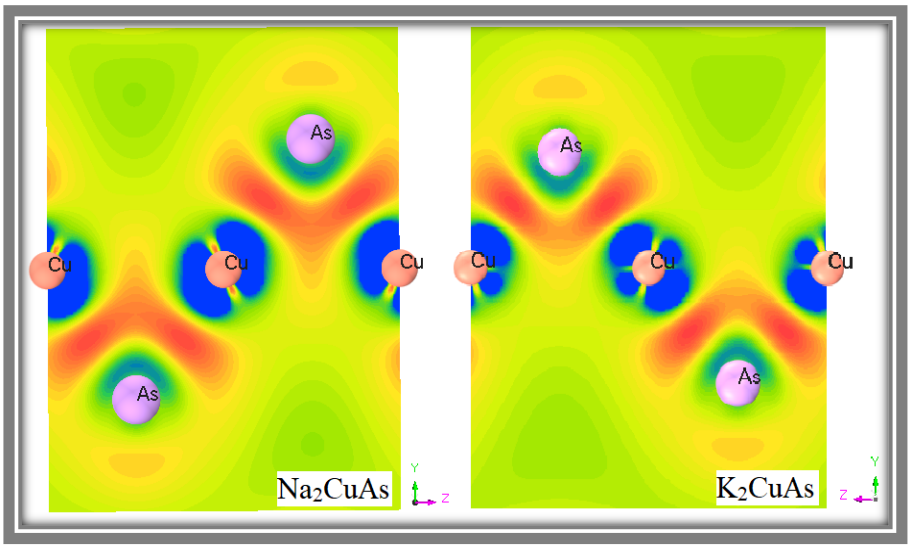

Figure III.9 *The cross-sections showing the Cu-As and Cu-Cu bonds for the A_2CuAs (A=Na, K) compounds.*

III.6 Optical Properties

Physical parameters such as the dielectric function $\varepsilon(\omega)$, the refractive index $n(\omega)$, the extinction coefficient $k(\omega)$, the reflectivity coefficient $R(\omega)$, and the absorption coefficient (α) are used to characterize the optical properties of a material. As mentioned in Chapter II, these properties may be theoretically computed from the dielectric function. The results of a purely predictive study conducted in the GGA-PBE approximation with a denser sampling grid of k points (16x16x16) thereby corresponding to 512 k points, will be presented and discussed in this section. The computed optical characteristics of *K_2CuAs* and *Na_2CuAs* along to the three propagation

directions of the incident wave *[100]*, *[010]* and *[001]*, are illustrated in **Figures III.10, III.11, III.12** and **III.13** for an energy range from *0eV* to *15eV* with small inner-range for visible domain from *1.63eV* to *3.26eV*.

The optical response functions are same in both directions *[100]* and *[010]*, but are clearly different in the *[001]* direction, as reported above. As a result, the herein considered materials are optically very anisotropic. This anisotropy becomes less marked at the higher energy part of the electromagnetic spectrum.

III.6.1 The dielectric function

The real portion of the dielectric function ε1(ω) defines the dispersion of electromagnetic radiation in the medium. The obtained zero frequency dielectric constant for Na_2CuAs (K_2CuAs) is 16.79 (8.87) When *E//[001]*, and 10.24(7.12) When *E//[100]* or *E//[010]*. ε1(ω) steadily grows from the zero-frequency limit to a maximum value in the lower visible spectrum for polarizations along the *[010]* and *[100]* directions for both materials. Then, ε1(ω) rapidly drops to negative values in the UV area, indicating that electromagnetic radiation is damped.

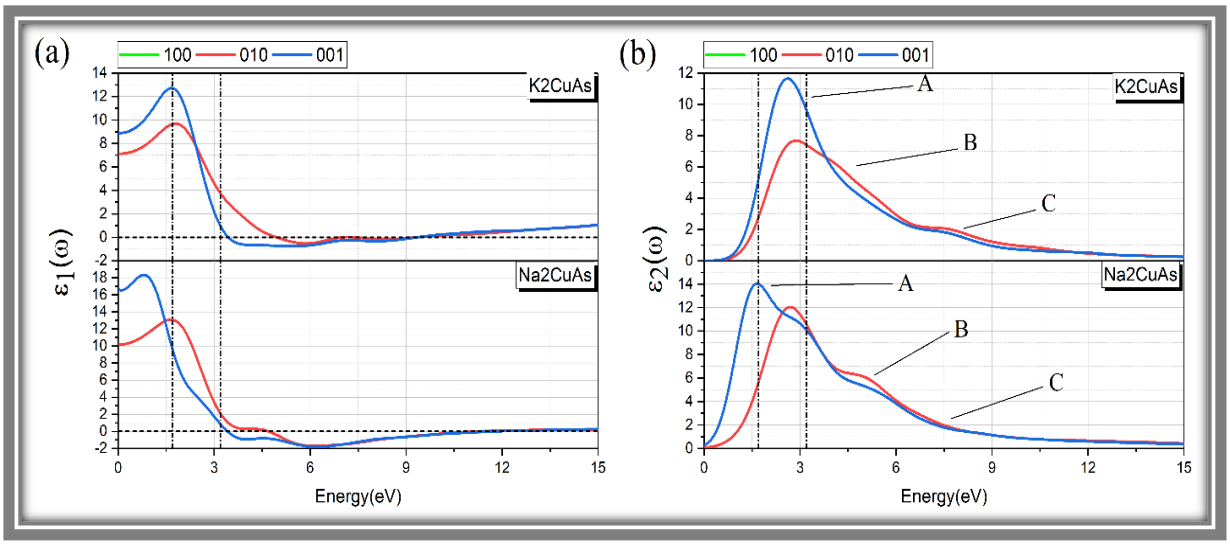

Figure III.10 *The spectra of the real (a) and imaginary (b) parts of the dielectric function as a function of the energy of the incident photon of the A_2CuAs (A = K or Na) compounds.*

The absorption in the material is linked to the imaginary part of the dielectric function. **Figure III.10** show the computed frequency dependent imaginary component of the dielectric function ε2(ω). For both materials, three well-resolved peaks, A, B, and C, can be observed. All three peaks

of *Na_2CuAs* (*K_2CuAs*) are mainly due to electronic transitions from the *Cu*-d states at the valance band to the *As*-p states at the conduction band. It is difficult to assign a specific transition to each peak due to the complexity of the band structure character around the Fermi level.

III.6.2 Refractive index and extinction coefficient

The fluctuations of the reflection index as a function of the energy of the incident photons are shown in **Figure III.11** The rather great closeness between the ε1(ω) and n(ω) curves is noteworthy. The zero frequency refractive index n(0) of *Na_2CuAs* (*K_2CuAs*) is anticipated to be 4.09 (2.97) when *E//[001]* and 3.20 (2.66) when *E//[010]* or *E//[100]*.

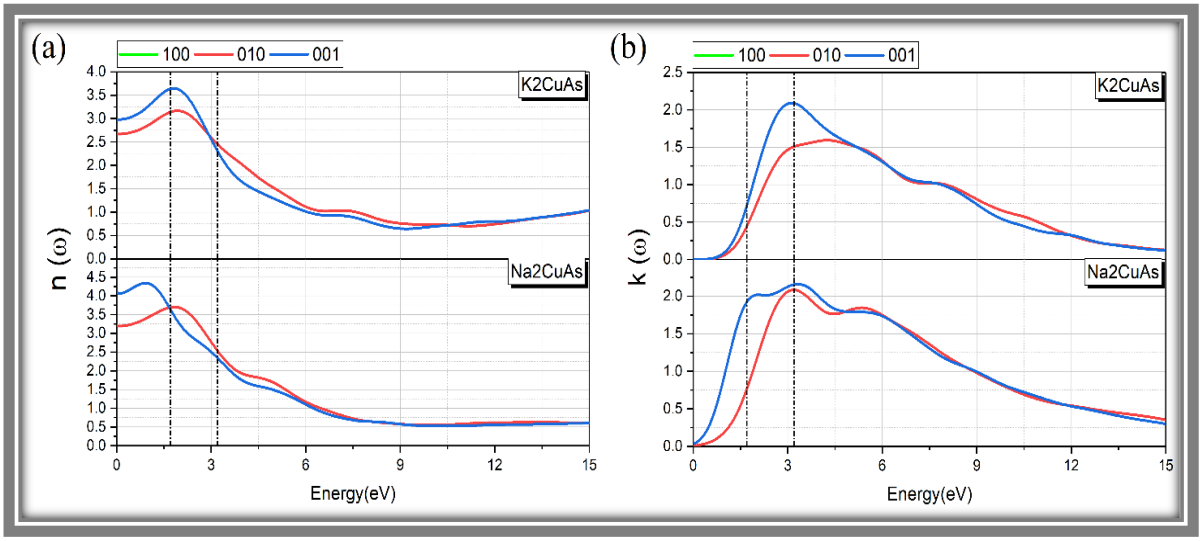

Figure III.11 *The refractive index spectra n (a) and the extinction coefficient k (b) as a function of the energy of the incident photon of the A_2CuAs (A=K or Na) compounds.*

Another optical measure that defines the attenuation of electromagnetic radiation in a given material is the extinction coefficient. Once more, the patterns of k(ω) and ε2(ω) have a striking resemblance. k(ω) grows quickly in the lower energy section to reach a maximum value at the lower part of the visible spectrum, then it drops slowly to rise its minimum values at the UV region.

III.6.3 Reflectivity

The R(ω) reflection coefficient describes the amount of energy reflected at the solid's interface. **Figure III.12** show the reflectivity spectra of the studied Zintl compounds. Both compounds show a nearly moderate and consistent reflectivity in an extended range of electromagnetic radiation starting from the zero-frequency limit to the extreme UV.

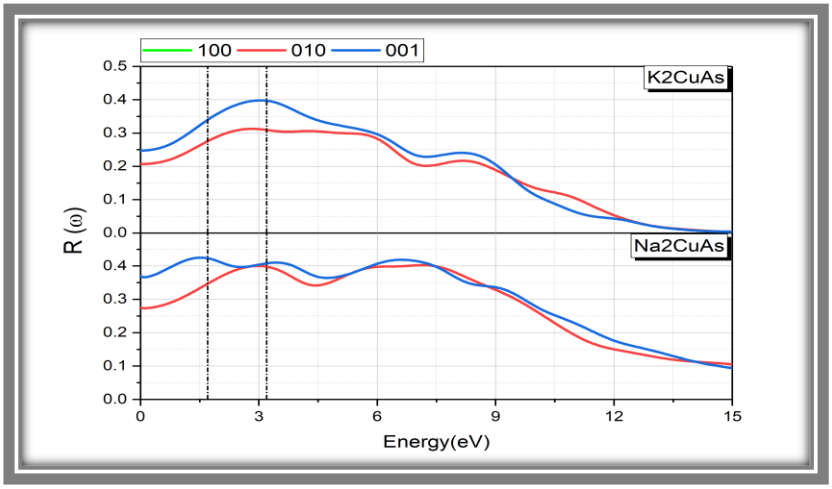

Figure III.12 *The spectra of the reflectivity as a function of incident photon's energy of the A_2CuAs (A = K or Na) compounds.*

III.6.4 The absorption coefficient

Figure III.13 show the frequency dependent absorption coefficients of *Na_2CuAs* and *K_2CuAs*, respectively. The acquired results reveal that both materials have a wide spread high absorption band in the extreme ultraviolet range, indicating that they may have optical activity in this region.

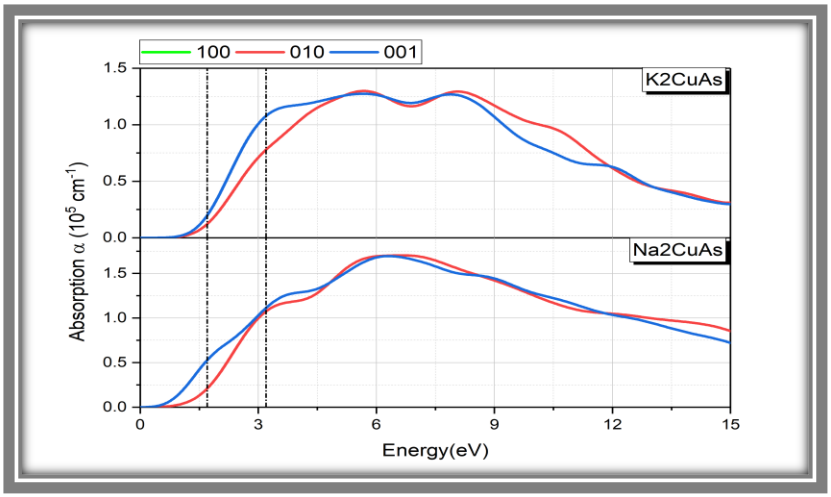

Figure III.13 *The spectra of the optical absorption as a function of the energy of the incident photon of the A_2CuAs (A = K or Na) compounds.*

References

1. **Vanderbilt, D., Soft.** *self-consistent pseudopotentials in a generalized eigenvalue formalism Physical Review B, 41(11): p. 7892-7895.* 1990.

2. **Koelling, D.D. and B.N. Harmon.** *A technic for relativistic spin-polarised calculations.* 1977 : s.n., Journal of Physics C: Solid State Physics, 10(16): p. 3107-3114.

3. **Monkhorst, H.J. and J.D. Pack.** *Special points for Brillouin-zone integrations. Physical review B, 13(12): p. 5188.* 1976.

4. **Hellmann, H.** *Einfüring in Quantumchemie (Franz Deuticke, Leipzig) 285 Feynman Phys. 56: p. 340.* 1937.

5. **Feynman, R.P.** *Forces in Molecules. Physical Review, 56(4): p. 340-343.* 1939.

6. **Savelsberg, G. and H. Schäfer.** *Darstellung und Kristallstruktur von Na2CuP, K2AgAs K2AgSb und K2AgBi/Preparation and Crystal Structure of Na2CuP, K2AgAs, K2AgSb, and K2AgBi. Zeitschrift für Naturforschung B, 32(7): p. 745-748.* 1977.

7. **Eisenmann, B., G. Savelsberg, and H. Schäfer.** *Zur Darstellung und Kristallstruktur von Na2CuAs, K2CuAs und K2CuSb. Zeitschrift für Naturforschung B, 31(10): p. 1344-1346.* 1976.

8. **Anglada, J.M. and J.M. Bofill.** *How good is a Broyden–Fletcher–Goldfarb–Shanno-like update Hessian formula to locate transition structures? Specific reformulation of Broyden–Fletcher–Goldfarb–Shanno for optimizing saddle points. Journal of computational chemistry 19(3): p. 349-362.* 1998.

9. **Shanno, D.F.** *Conditioning of quasi-Newton methods for function minimization. Mathematics of computation, 24(111): p. 647-656.* 1970.

10. **Caro, M.A., S. Schulz, and E.P. O'Reilly.** *Comparison of stress and total energy methods for calculation of elastic properties of semiconductors. Journal of Physics: Condensed Matter, 25(2): p. 025803.* 2012.

11. **Mouhat, F. and F.-X. Coudert.** *Necessary and sufficient elastic stability conditions in various crystal systems. Physical Review B, 90(22).* 2014.

12. **Born, M.** *On the stability of crystal lattices. I. Mathematical Proceedings of the Cambridge Philosophical Society, 36(02).* 2008.

13. **Voigt, W.** *Lehrbuch der kristallphysik (mit ausschluss der kristalloptik). Leipzig; Berlin; [Ann Arbor, Mich.]: B.G. Teubner [J.W. Edwards]*. 1946.

14. **Reuss, A.** *Berechnung der fließgrenze von mischkristallen auf grund der plastizitätsbedingung für einkristalle. ZAMM-Journal of Applied Mathematics and Mechanics/Zeitschrift für Angewandte Mathematik und Mechanik, 9(1): p. 49-58.* 1929.

15. **Hill, R.** *The elastic behaviour of a crystalline aggregate. Proceedings of the Physical Society Section A, 65(5): p. 349.* 1952.

16. **Chen, X.-Q., et al.** *Modeling hardness of polycrystalline materials and bulk metallic glasses Intermetallics, 19(9): p. 1275-1281.* 2011.

17. **Pugh, S.F.** *XCII. Relations between the elastic moduli and the plastic properties of polycrystalline pure metals. The London, Edinburgh, and Dublin Philosophical Magazine and Journal of Science, 45(367): p. 823-843.* 2009.

18. **Lakes, R.** *Foam structures with a negative Poisson's ratio. Science, 235: p. 1038-1041.* 1987.

GENERAL CONCLUSION

General Conclusion

This work is a contribution to study the structural, elastic, electronic and optical properties of the Zintl compounds K_2CuAs and Na_2CuAs. Relevant bibliographic research has shown us that very little is known about the physical properties of these materials. In response to the lack of studies on such important topic, we set ourselves the goal of creating a reliable knowledge base from a series of ab-initio simulations based on density functional theory (DFT) and the pseudopotential approach as implemented in the CASTEP code. The GGA-PBE generalized gradient approximation is used to process the exchange-correlation potential.

The adopted calculation methodology accurately reproduces these materials equilibrium geometry. The computed elastic constants show that the two materials are mechanically stable in the orthorhombic structure (SG Cmcm N °: 63). The bulk modulus B and shear modulus G are both low, indicating that the materials under consideration are soft and easily compressible. The anisotropic elastic response is shown by the directional dependence of Young's modulus and linear compressibility, as well as the computed anisotropy indices. Both materials have poor thermal conductivities and heat capacity, based on the estimated low Debye temperatures.

The estimated energy band structures in the GGA-PBE approximation reveal that these materials are narrow indirect band gap semiconductors. The strong covalent nature of the *Cu-As* bond in the zigzag chains along the c axis, as well as the ionic character of the *A(K/Na)-Cu* bond, are readily confirmed by the Mulliken populations and the electron density difference maps.

Many optical parameters have been computed for a large spectral range of 0 to 15 eV. According to our findings, these two compounds should be transparent in the infrared region and active in the UV limit by evidence of a broad optical absorption band at this region.

Our findings can be used as a reference for future research because there have been no previous experimental investigations on the physical characteristics of these polar intermetallic.

Finally, we hope that our work may open up new perspectives for research into these materials.

Abstract

The ground state physical properties of Zintl compounds Na_2CuAs and K_2CuAs have been investigated. Using the GGA-PBE approximation of density functional theory (DFT) as implemented in the CASTEP code. The calculated equilibrium geometry agrees well with its experimental counterpart. The computed elastic stiffness constants were used to investigate the whole elastic behavior of the compounds under consideration. According to the obtained results, both materials will show high extend of elastic anisotropy; they are soft and easily compressible. The energy band dispersion indicates that they are indirect narrow gap semiconductors. Mulliken charges analysis show that there is a significant covalent interaction between *Cu* and *As*, as well as ionic interaction of *A-Cu* contact. Many important optical properties have been computed throughout a broad energy range. According to the obtained results, both materials are active in the UV spectral domain and transparent in the IR.

Keywords: Density functional theory, pseudopotentials, planes wave, generalized gradient approximation, structural properties, elastic properties, optical properties, semiconductors, Zintl phase.

ملخص

تم فحص الخصائص الفيزيائية للحالة الأساسية لمركبات الزنتل Na_2CuAs وK_2CuAs وفقا لتقريب التدرج المعمم GGA-PBE لدالية الكثافة الالكترونية المدرجة في برنامج المحاكات الرقمية CASTEP. في ضل المقاربة النظرية المعتمدة، توافقت البنية البلورية للحالة الاساسية جيدًا مع نظيرتها التجريبية . استخدمت ثوابت الصلابة المحسوبة لفحص السلوك المرن للمركبات قيد الدراسة. اظهرت النتائج ان كلتا المادتان هشتان وسهلتا الانضغاط تميزهما درجة عالية من عدم تماثلية المناحي المرونية. يشير تشتت نطاق الطاقة الكترونية لهذه المواد إلى أنها أشباه موصلات ذات فجوة طاقة ضيقة غير مباشرة. يظهر تحليل موليكان أن الرابطة بين ذرات النحاس و الآرسونيك تساهمية غالبا خلافا للرابطة بين الصوديوم او البوتاسيوم و النحاس التي تبين لنا انها ايونية صرفة. في هذا العمل تنبأنا كذلك بالعديد من الخصائص البصرية للمواد المذكورة آنفا في نطاق طيفي واسع. وقد اظهرت النتائج انها نشطة لدى تعريضها الاشعة الفوق بنفسجية وشفافة في نطاق الاشعة تحت الحمراء.

كلمات مفتاحية : نظرية دالية الكثافة, أشباه الكمونات, الأمواج المستوية, تقريب التدرج المعمم , الخصائص البنيوية, الخصائص المرونية,الخصائص الضوئية أشباه الموصلات, اطوار Zintl

Résumé

Les propriétés physiques de l'état fondamental des composants Zintl Na_2CuAs et K_2CuAs ont été étudiées. Les propriétés structural, élastiques, électroniques et optiques sont étudiées moyennant la théorie fonctionnelle de la densité et l'approximation du gradient généralisé GGA-PBE implémentées dans code CASTEP. La géométrie d'équilibre à l'état fondamentale est en parfait accord avec son homologue expérimentale. Les constantes de rigidité élastique calculées ont été utilisées pour étudier le comportement élastique des composés considérés. Les deux matériaux sont souples et facilement compressibles. Ils sont caractérisés par un degré élevé d'anisotropie élastique. La dispersion des bandes d'énergie de ces matériaux indique qu'il s'agit de semi-conducteurs à faibles gaps indirects. L'analyse des populations de Mulliken montre qu'il existe une liaison covalente forte entre les atomes du cuivre et d'arsenic, ainsi qu'une liaison ionique entre le métal alcalin est le cuivre. Plusieurs paramètres optiques importants ont été calculés dans une large gamme spectrale. Les deux matériaux sont actifs dans le domaine des UVs et transparents dans l'IR.

Mots clés : Théorie fonctionnelle de la densité, pseudo-potentiels, ondes planes, approximation du gradient généralisé, propriétés structurales, propriétés élastiques, propriétés optiques, semiconducteurs, phases Zintl, intermétalliques polaires.